



**HAL**  
open science

# State-of-the-art in the mechanistic modeling of the drying of solids: A review of 40 years of progress and perspectives

Patrick Perré, Romain Rémond, Giana Almeida, Pedro Augusto, Ian Turner

## ► To cite this version:

Patrick Perré, Romain Rémond, Giana Almeida, Pedro Augusto, Ian Turner. State-of-the-art in the mechanistic modeling of the drying of solids: A review of 40 years of progress and perspectives. *Drying Technology*, 2023, pp.1-26. 10.1080/07373937.2022.2159974 . hal-03922881

**HAL Id: hal-03922881**

**<https://hal.science/hal-03922881>**

Submitted on 4 Jan 2023

**HAL** is a multi-disciplinary open access archive for the deposit and dissemination of scientific research documents, whether they are published or not. The documents may come from teaching and research institutions in France or abroad, or from public or private research centers.

L'archive ouverte pluridisciplinaire **HAL**, est destinée au dépôt et à la diffusion de documents scientifiques de niveau recherche, publiés ou non, émanant des établissements d'enseignement et de recherche français ou étrangers, des laboratoires publics ou privés.

# State-of-the-art in the mechanistic modeling of the drying of solids: a review of 40 years of progress and perspectives

Patrick Perré<sup>a,b,\*</sup>, Romain Rémond<sup>c</sup>, Giana Almeida<sup>d</sup>, Pedro Augusto<sup>b</sup>, Ian Turner<sup>e</sup>

<sup>a</sup>Université Paris-Saclay, CentraleSupélec, LGPM, Gif-sur-Yvette, France

5 <sup>b</sup>Université Paris-Saclay, CentraleSupélec, LGPM SFR Condorcet FR CNRS 3417, Centre Européen de Biotechnologie et de Bioéconomie (CEBB), 3 rue des Rouges Terres 51110 Pomacle, France

<sup>c</sup>LERMAB, ENSTIB, Université de Lorraine, 88 000 Epinal, France

<sup>d</sup>SayFood, AgroParisTech, Université Paris-Saclay, 91 120 Palaiseau, France

<sup>e</sup>School of Mathematical Sciences, Queensland University of Technology, Brisbane, Australia

---

## 10 Abstract

This review paper was written on the occasion of the 40<sup>th</sup> anniversary of the *Drying Technology Journal*. Interestingly, most of the progress made in the domain of drying modeling and simulation has occurred over the last 40 years. Indeed, 40 years ago, the comprehensive formulation of coupled heat and mass transfer in porous media was available, however its potential use for  
15 computational simulation was only in its nascent stage. This is therefore an ideal time span in which to take a full historical context, to present the state-of-the-art and to give insights into its future trajectory. All aspects are deliberately presented in a pedagogical manner with many illustrations to make the text accessible to young scientists. However, for the benefit of experts, detailed formulations are provided in the annexes. The main points addressed in this work include:

- 20 • The description of the comprehensive macroscopic formulation,
- An historical perspective of the progress made in computational simulation,
- The contribution of modeling in parameter characterization,
- The mechanical aspects of drying: strain and stress induced by drying, including the case of large deformations,
- 25 • The impact of non-local equilibrium,
- The promising domain of the digital twin in parameter tuning and control/command.

*Keywords:* applied mathematics, digital twin, machine learning, mechanics, multiphysics, multiscale, transfers

---

## 1. Introduction

30 Drying is a complex process involving many coupled and non-linear thermal, physical, mechanical, chemical and biological phenomena (Fig. 1). As primary effects, coupled heat and mass transfer are involved within and around the product. Following these coupled transfers, spatial fields of moisture content (MC) and temperature develop inside the product. Understanding these transfer aspects is the primary objective of most works  
35 published in the field of drying because they enable useful indicators of the drying process to be addressed, such as the drying time, the effect of product size, and the energy consumption. The drying quality could be partly addressed as well, for example the chemical degradation due to the coupled effect of hydric and thermal activation over time. Due to

---

\*Corresponding author

Email address: [patrick.perre@centralesupelec.fr](mailto:patrick.perre@centralesupelec.fr) (Patrick Perré )

the strong coupling and the non-linear behavior, analytic solutions are available only under strong and somehow unrealistic assumptions : computational simulation is therefore mandatory.

Deformation, internal stress, product failure (collapse, checking) and poor re-hydration are among the major challenges encountered in the drying process. Addressing these aspects required the domain of solid mechanics to be added to extend the formulation. The driving force for stress development and deformation is the shrinkage induced by water removal. Due to the moisture content profiles, this field does not fulfill compatibility conditions, which triggers the development of drying stresses. Over time, shrinkage occurs with the presence of internal stresses, which induces a strong mechanical behavior to evolve spatially due to the local values of MC and temperature: this gives rise to the well-known problems of casehardening and stress reversal, which is a major challenge for some products such as wood and clay. In the case of biological materials, their inherent anisotropy and heterogeneity adds another layer of complexity in this evaluation: each of the tissue and cell layers are unique in composition, structure and, thus, properties (from the resistance to water permeation, passing through the equilibrium moisture, until their mechanical properties, thus affecting shrinkage).

Finally, figure 1 depicts the key factors likely to impact the quality of the dried product. Modeling these complementary, but strongly coupled, domains (transfer, mechanics and additional phenomena) provides a comprehensive and in-depth view of the process: time, cost, and economical value. One could dream at an ideal simulation tool that is able to account for all these coupled transport phenomena, allowing the effect of each parameter to be investigated and the whole process to be improved or even optimized as a function of the expectations of the end-users. However, to achieve this ultimate objective is a long and difficult route. In the following sections, each discussion point will be addressed with an historical perspective to present the state-of-the-art of the domain. Finally, a conclusion section will be given to summarize the open questions and the promising prospects for tackling the remaining challenges.

## 2. The comprehensive macroscopic formulation

After the pioneering modeling research undertaken in the 50s and 60s [38, 84, 45], the comprehensive set of macroscopic equations governing coupled heat and mass transfer in porous media were rigorously derived in the 70s using the method of volume averaging [105, 26, 123, 124]. The development of the volume-averaged transport equations requires the existence of a representative elementary volume (REV)  $V$  that is sufficiently large to smooth the microscopic fluctuations and sufficiently small to avoid macroscopic variations. Two averaging operators are defined on this REV, namely, the superficial average (also called global average) and the intrinsic average. For example, the superficial average of the density of the liquid phase is given by

$$\bar{\rho}_w = \frac{1}{V} \int_{V_w} \rho_w dV, \quad (1)$$

and the intrinsic average is expressed as

$$\bar{\rho}_w^w = \frac{1}{V_w} \int_{V_w} \rho_w dV, \quad (2)$$

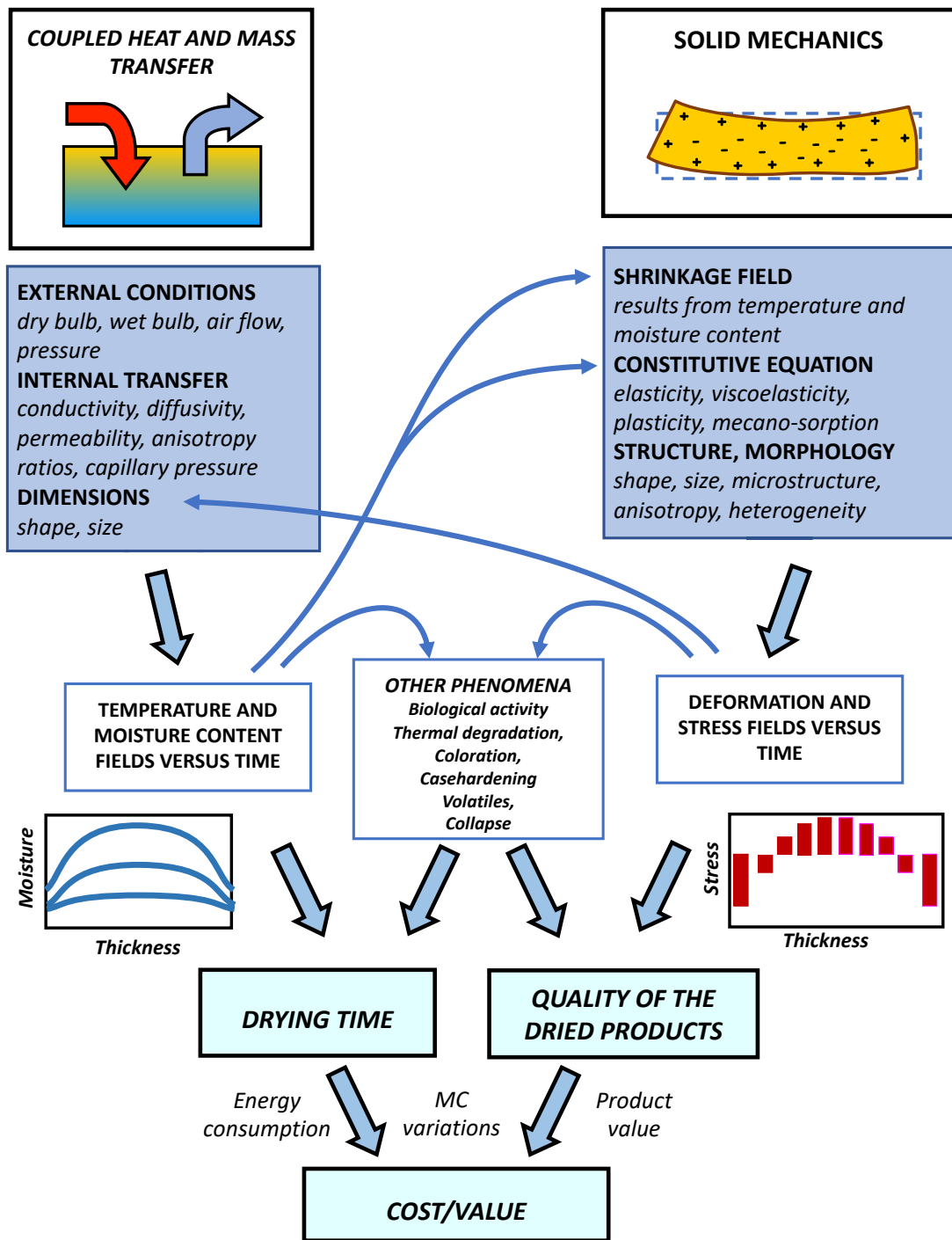


Figure 1: An overview of the intricate mechanisms involved in drying: a typical multiphysics problem.

80 where  $V_w$  is the volume of the liquid phase contained in  $V$ . Further, the relationship  $\bar{\rho}_w = \varepsilon_w \bar{\rho}_w^w$  in which  $\varepsilon_w = V_w/V$  is the volume fraction of the liquid phase.

The full set of equations proposed in [123, 7, 124] and later adapted to the case of hygroscopic products [68, 71], can be considered as the state-of-the-art in terms of the macroscopic formulation. It includes three state variables (for example moisture content, temperature and total pressure) and is able to describe most drying processes, including those which give rise to an internal over-pressure (high temperature drying, vacuum drying, microwave drying).

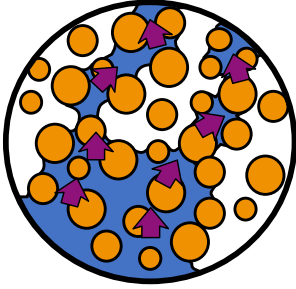
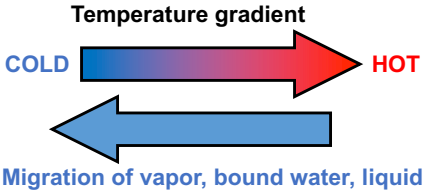
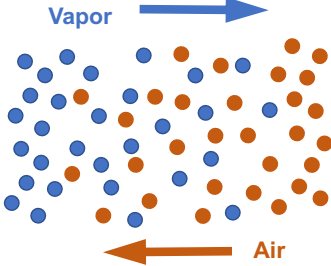
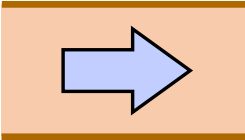
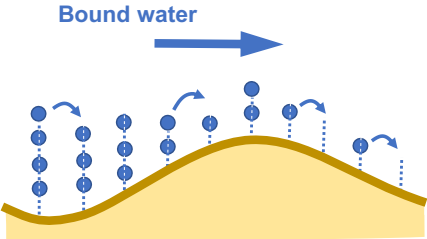
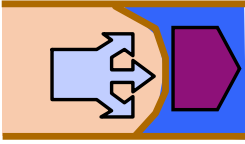
90 For this review paper, our preference was to put the full details of the mathematical formulation in annex A, and hereafter we will describe all the physics embedded in these equations. Each of the different physical mechanisms involved in the moisture migration phenomena is summarized in table 1. The left column of this table lists the three modes of migration inside a solid induced by a gradient of MC:

- 95 • Liquid migration is driven by capillary pressure. The gradient of capillary pressure develops because the meniscus radii decreases with MC, which increases the pressure gap between the gaseous and liquid phases. The moisture flux equals the product of the gradient of capillary pressure with the liquid phase mobility (ratio of the liquid permeability and the liquid viscosity) (equ. A.5)
- 100 • Binary diffusion is crossed diffusion of water vapor and air in the gaseous phase, when the latter exists. When considering mass balance equations, the driving force is the gradient of mass fraction [8] and the vapor flux equals this gradient times the effective diffusivity (equ. A.1)
- 105 • Bound water migration occurs when water molecules that are more or less bound to the solid are able to migrate. Different driving forces have been proposed in the literature. The bound water flux equals the gradient of this driving force times the bound water diffusivity (equ. A.6)

In addition to these MC gradient-triggered moisture fluxes, additional mechanisms may be involved. Depending on the configuration, these effects can be of crucial importance, even accounting for most of the moisture flux.

- 115 • Thermo-migration refers to a flux of moisture induced by a gradient of temperature. This is very likely to occur in a solid during drying. Due to the effect of pressure on saturated vapor pressure, the temperature level acts directly on the mass fraction, even though the effect is reduced in the hygroscopic range, hence on its gradient and on binary diffusion. Note also that capillary pressure is affected by the temperature level though its effect on the surface tension. Finally, it was reported for wood that a temperature gradient induces a flux of bound water. [104, 9, 49]. This explains why the choice of driving force for bound water migration is important for configurations with large temperature gradients.
- 120 • In the case of a high temperature configuration, the effect of temperature on the saturated vapor pressure is such that the internal partial pressure of vapor can exceed the external pressure. Consequently, it would exceed in the domain of liquid water. This is the case for high temperature drying (above 100°C), or for vacuum drying.

Table 1: The different physical mechanisms able to drive moisture in a solid.

| Gradient of moisture as driving force   | Other driving forces   |
|---|--|
| <p data-bbox="376 412 644 443"><b>Capillary migration</b></p> <p data-bbox="242 461 778 582">Liquid water migrates from zones with large MC, hence large menisci to zones with low MC, where suction is larger due to smaller menisci.</p>   | <p data-bbox="948 412 1200 443"><b>Thermo-migration</b></p> <p data-bbox="807 461 1343 645">Temperature increases water vapor migration (effect of T on <math>P_{vs}</math>), lowers capillary pressure (effect of T on surface tension) and activates bound water. Whatever the nature of water, moisture always migrates from hot zones to cold zones.</p>                                       |
| <p data-bbox="399 922 622 954"><b>Binary diffusion</b></p> <p data-bbox="242 972 778 1061">In the gaseous phase, binary diffusion takes place. The driving force is the gradient of molar or mass fraction.</p>    | <p data-bbox="938 922 1209 954"><b>Convection of vapor</b></p> <p data-bbox="807 972 1343 1155">In <b>high temperature configurations</b>, the internal temperature can be higher than the external boiling point of water. A gradient of total gaseous pressure develops, which is an efficient driving force to enhance vapor transport (together with air) by Darcy's law.</p>                |
| <p data-bbox="357 1370 660 1402"><b>Bound water diffusion</b></p> <p data-bbox="242 1420 778 1572">Bound water molecules can jump from one sorption site to the other. This is a statistical behavior activated by both temperature and MC (the molecules mobility increases for less bound molecules).</p>  | <p data-bbox="935 1370 1216 1402"><b>Convection of liquid</b></p> <p data-bbox="807 1420 1343 1639">In the presence of a gradient of total gaseous pressure (<b>high temperature configuration</b>) and when MC is still high, the gaseous pressure can act on menisci to drive liquid water. The driving force is the gradient of liquid pressure (gaseous pressure - capillary pressure).</p>  |

125 Similar effects can occur more readily with a large internal source of heat, such as in  
microwave of high frequency heating. A gradient of total gaseous pressure can act  
both on the vapor flux through Darcy's law, accounting for the permeability to the  
gaseous phase (equ. A.4), or through the effect of gaseous pressure on the liquid  
pressure, accounting for the permeability to the liquid phase (equ. A.5).

130 Heat transfer is not represented in table 1. In spite of their heterogeneity, the classical  
Fourier's law stands at the macroscopic level, with an effective thermal conductivity that  
depends of phase morphology and phase properties. It is also important to recall that,  
in a porous medium, heat transfer can also occur, very efficiently, by enthalpy transfer :  
evaporation - migration - condensation.

### 135 3. The coupling between heat and mass transfer

#### 3.1. Low temperature configuration

During drying, all these mechanisms act simultaneously in a coupled manner. Figure 2  
provides a conceptualization of this coupling during two important periods of a convec-  
tive drying process. Assuming the exchange surface of the product remains in the domain  
140 of liquid water for a certain period, a constant drying rate period takes place after an ini-  
tial, short, transient thermal regime. During this period, the vapor pressure at the surface  
remains equal to the saturated vapor pressure. The solid therefore equilibrates at the wet  
bulb temperature. Transfers in the boundary layers allow crossed fluxes of heat towards  
the medium and water vapor from the exchange surface. As moisture leaves the product  
145 as vapor, the heat provided to the product is entirely used to supply the latent heat of  
evaporation. The external drying conditions impose the values of temperature and va-  
por pressure outside the boundary layer, while the gas velocity, together with geometry,  
define the heat and mass transfer coefficients. Consequently, the drying rate depends on  
external conditions only, which explains why the first drying stage is also called the con-  
stant drying rate (CDR) period.  
150

During this period, water is supplied to the exchange surface by capillary migration : re-  
gions of large MC have larger menisci between the liquid and gaseous phases, hence a  
small capillary pressure (Right drawing of figure 2). The ability of the internal structure  
155 of the medium to drive liquid towards the surface, together with the product geome-  
try, defines the duration of the constant drying rate period. This phase ends once the  
vapor pressure is no longer equal to the saturated vapor pressure. From this point on-  
wards, the drying rate decreases and the product temperature gradually increases. The  
driving forces across the boundary layers are progressively reduced, which signifies the  
commencement of the decreasing drying period. One zone develops from the surface, in  
160 which moisture migrates by a combination of gaseous and/or bound water diffusion. To  
allow for vapor diffusion, liquid should be changed to vapor inside the product : one part  
of the heat provided at the surface continues to move inwards through the medium by  
thermal diffusion to supply the latent heat of evaporation where liquid evaporates.

165 Throughout the process, the coupling between heat and mass transfer is essential : any  
water removed from the product needs its latent heat of evaporation, and eventually the  
differential heat of sorption, to be supplied somewhere.

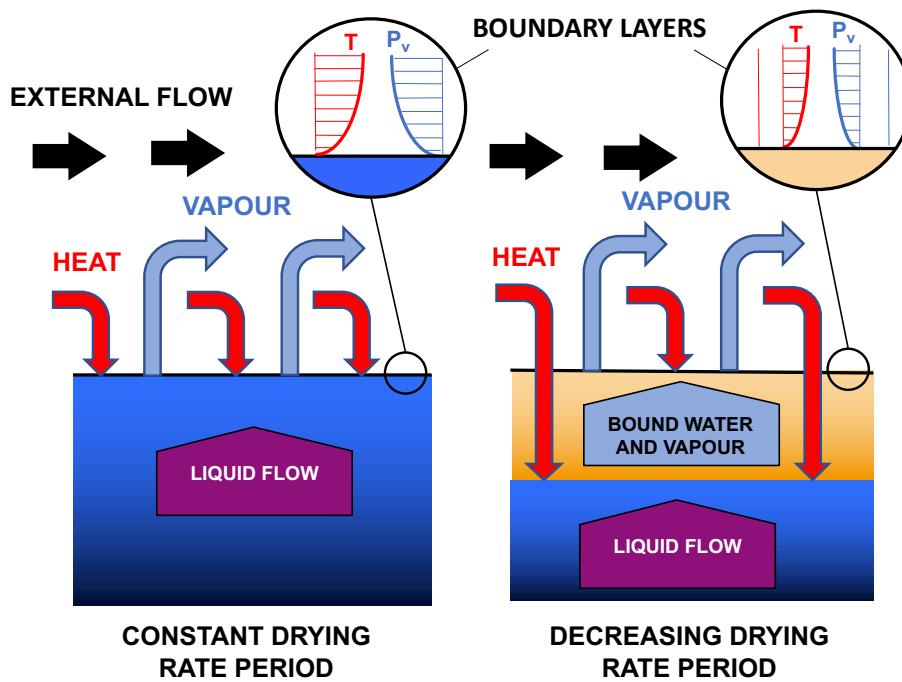


Figure 2: A graphical summary of the coupled transfer phenomena involved in drying.

### 3.2. High temperature configuration and internal heating

170 The former description corresponds to a "low temperature" configuration. A very efficient driving force can be triggered in a "high temperature" configuration. Such configurations correspond to drying conditions in which the vapor pressure exceeds the external pressure somewhere in the product during the process. This is the case if the temperature exceeds the boiling point with a water activity equal to the unit (presence of liquid water) or if the temperature level is such that the saturated vapor pressure compensates for the local water activity. This gives rise to an internal overpressure, hence a pressure gradient able to drive moisture either as liquid, by acting on menisci (the gaseous pressure changes the liquid pressure) or as vapor, simply through the Darcy's law (see table 1).

180 These temperature levels can be achieved by providing sufficient heat to the surface of the product. This can be obtained by convective drying at a temperature higher than 100°C at atmospheric pressure or higher than the corresponding boiling point of water in vacuum drying. The later is particularly interesting for product prone to thermal degrade, as high temperature configuration can be obtained at temperatures much lower than 100°C. Radiative heating is also likely to give rise to "high temperature" drying. When heat is provided at surface, it must then be driven inwards by thermal conduction. This has two drawbacks:

- A thermal gradient is required to reach the desired core temperature. This is restrictive for large products as the resistance to heat transfer increases with thickness and a compromise must be found between the heat flux, hence the drying rate, and the increase in surface temperature,

- The thermal gradient is oriented outwards (surface temperature larger than core temperature), while the the MC gradient is oriented inwards (MC at the core is larger than the surface MC). These two gradients act in opposite ways for moisture migration. This means that the primary effect of MC gradient is partly counterbalanced by thermal migration.

Internal heating is a clever way to overcome these drawbacks of conventional high temperature drying. Heating the core of the product directly not only cancels the resistance to thermal conduction, but also gives rise to a positive temperature gradient that allows water to exit by thermo-migration (see the different thermo-migration mechanisms described in the previous section). Conventional means of achieving internal heating include the use of microwaves or high frequencies. In this case, a source term should be involved in the enthalpy equation (term  $\varphi$  in equations A.2 and A.9). This source term varies in space and in time, as a result of the permittivity fields (real and imaginary values, functions of the material, its temperature and moisture content) and the boundary conditions. It can be evaluated by simple approaches [19, 4] or by solving Maxwell equations [115, 70, 128]. Once the source term is computed, the full macroscopic set of equations is perfectly able to predict the increase in internal pressure and its very efficient effect on moisture migration.

As final comment, it is important to mention that the internal heating can be very efficient even when the heat source is not sufficient to switch to a "high temperature" configuration. Drying with a slight internal heat source is likely to reverse the temperature gradient and is able to increase significantly bound water and vapor migration, even at moderate temperatures. This strategy has been successfully applied to the drying of oak, a wood species very difficult to dry and which collapses at high temperature [12, 92].

Figure 3 summarizes these different situations. In classical drying at low temperature, heat is supplied to the surface, which is warmer than the core. The thermal gradient, through thermo-migration, acts against the moisture gradient. Large MC gradients are needed to drive moisture from center to surface (Fig. 3A). Internal heating allows this thermal gradient to be reversed, even when remaining in a low temperature configuration. Both gradients (temperature and moisture content) drive moisture towards the surface, which flattens the MC profiles (Fig. 3B). When the heat supplied at the surface of the product is sufficient to increase the internal temperature above the boiling point, a gradient of total gaseous pressure develops, which adds a very efficient driving force to move moisture to the surface. The MC profiles are seriously flattened and could even be reversed if the liquid water is mobile enough (Fig. 3C). Finally, an intense internal heating accumulates all advantages : positive thermal gradient plus the efficiency of a gradient of total gaseous pressure. This the best coupling of heat and mass transfers that can be imagined for an efficient moisture migration (Fig. 3D).

#### 4. Computational solution of coupled transfers

The computational modeling of the drying process has undergone significant advancements over the last forty years. In the 80s, only very simplistic drying models were solved. Typically, these were one-dimensional, single equation models, which in many cases did

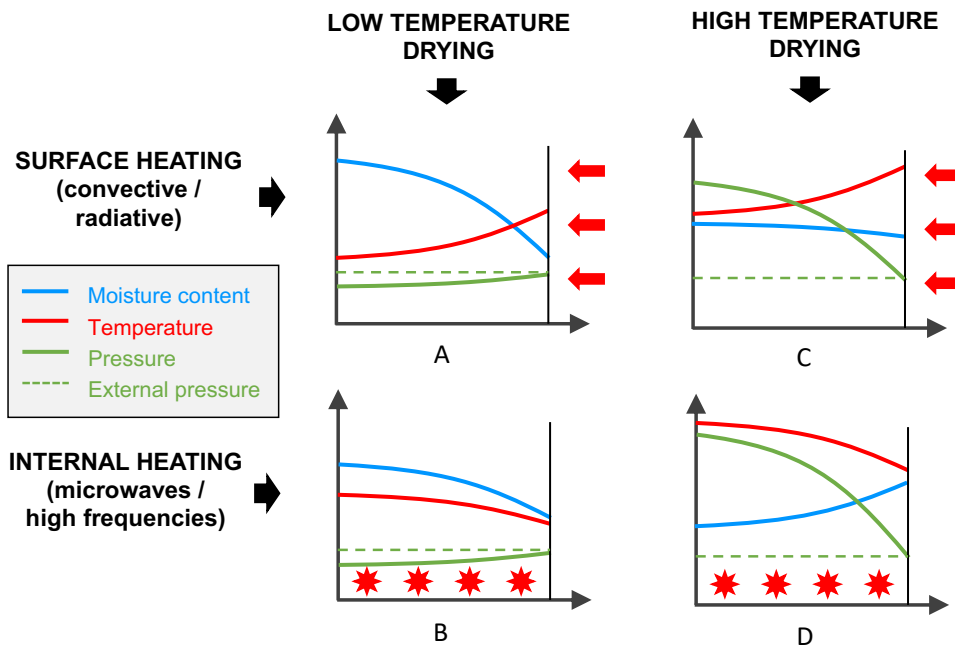


Figure 3: Schematic representations of temperature, moisture content and pressure profiles as a function of two drying characteristics : low temperature *vs* high temperature and surface heating *vs* internal heating.

not consider the crucial coupling that exists between the heat and mass transfer phenomena. Focusing on one of the models proposed at that time which did take this coupling into account, Sharp [102] published a modeling review for a deep bed of grains. Simple models, using the assumption of equilibrium, were also used at that time to obtain reasonable simulation times. The first comprehensive simulation codes for solving the spatio-temporal evolution of the MC, temperature, and internal pressure fields with full coupling were published in the 80s [11, 106, 61]. The first papers using a 3-variable formulation that were able to compute the internal pressure and its effect on heat and mass transfer, were published in the same period [89, 56, 31, 87].

Over the decades, the tremendous increase of computer power together with the use of efficient mathematical solvers completely changed the situation : several hours of CPU time was needed in the late 80s to solve the 3-variable model in 1D, while 0.1s is now sufficient. In fact, nowadays, it is possible to compute the transport phenomena across a range of different spatial and temporal scales [13, 15] from the micro (cell) through to the dryer level, and this has led to breakthroughs in the fundamental understanding of the underlying processes. This new knowledge has identified ways to optimize existing drying operations, and to investigate the potential of new drying technology.

We must keep in mind that the advancement in the solution of the macroscopic formulation is due to two important factors. The first is undoubtedly a result of the substantial increased computing power that has become available over this period. For example, in 1985, the supercomputer Cray-2 had a power of 1.9 GFlops (Giga =  $10^9$ , Flops = floating

point operations per second) and in 2022 the No. 1 system of the actual TOP500 (release  
260 of June 2022) has a peak power over one EFlops (Exa =  $10^{18}$ ). Regarding processors for  
personal computers, the intel 386 launched in 1985 was incapable of reaching one MFlops  
(Mega =  $10^6$ ). Nowadays, the most powerful processors reach the TFlop (Tera =  $10^{12}$ )  
range, and this figure is much higher for GPUs (of this order of 100 TFlops). In both cases,  
it is about a hundred million-fold increase in computing power over four decades.

265 However, this impressive increase should not mask the second factor, which is due to  
the development of innovative numerical algorithms for the rapid solution of the highly  
non-linear, coupled, multi-phase heat and mass transfer equations that govern the drying  
process. In a recent paper, Thompson *et al.* [111] analyzed five application areas where  
270 computation is critical, including weather forecasting, oil exploration, and protein folding.  
They found that increases in computing power explains between 49%–94% of the overall  
performance improvements observed in these research fields and, most interestingly, they  
identified that an exponential increase in computing power was needed to obtain linear  
improvements in outcomes for these areas. As an example, Thompson *et al.* [111] mention  
275 that in weather forecasting there has been a *trillion-fold* increase ( $10^{12}$ ) in the amount of  
computing power over the last 4-5 decades, and this increased computer power has led to  
improvements in the accuracy of three-day temperature predictions by one-third of a de-  
gree. However, this improvement is not achieved by just running existing codes on faster  
computers; instead algorithms must be continuously re-engineered to take advantage of  
280 increased computer power, and it is this human ingenuity that proves vital not only for  
improving performance, but also for harnessing the ever-more-powerful computing en-  
gines that are now readily available for driving scientific research. These observations are  
most likely also true in the field of drying.

285 Typically, the underlying governing drying conservation laws are discretized in space us-  
ing either finite difference, finite volume, or finite element methods. The full Newton-  
Raphson method was a first efficient step, compared to the originally used fixed-point  
relaxation methods [60], to solve non-linear and coupled equations [126, 113]. Thanks  
to these methods, together with the improvement of computer power, the first papers de-  
290 scribing computational drying models in 2D and 3D settings appeared in the literature  
from the 1990s [76, 114, 68, 33, 32, 101]. These additional space dimensions are particu-  
larly needed to obtain realistic simulations when simulating strongly anisotropic media,  
such as wood, in high temperature drying configurations. In such situations, one or two  
dimensions can be mainly devoted to transfer by conduction the latent heat of vapor-  
295 ization to the medium while moisture migrates along the strongly permeable direction  
due to a gradient of total pressure. For the sake of example, a 2D simulation of wood  
drying at high temperature was computed using the drying software *TransPore* (Fig. 4).  
The dry and wet bulb temperature are respectively at  $140^{\circ}\text{C}$  and  $80^{\circ}\text{C}$ . Consequently, the  
CDR period, occurring at  $80^{\circ}\text{C}$ , is a low temperature configuration. The situation changes  
300 completely during the decreasing drying rate : the board temperature increases and even-  
tually exceeds the boiling point. An overpressure develops inside the board that drives  
liquid along the highly permeable longitudinal direction, the direction of sap ascent in  
the tree, up to the endpiece. The drying time of 6 hours selected in figure 4 corresponds  
to this period. The ability of the comprehensive set of equations to solve transfer mecha-  
305 nisms in the presence of an internal heat source is part of the great success of the physical

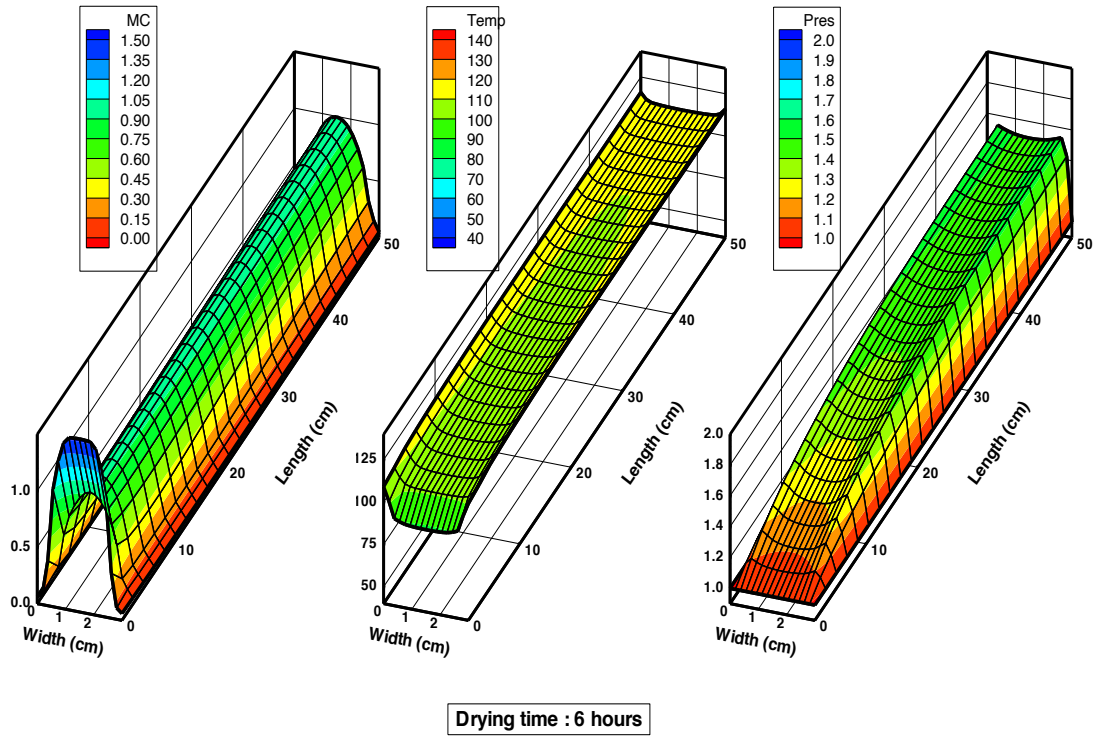


Figure 4: Example of 2D simulation at high temperature of a board of wood. The development of an internal overpressure during the decreasing drying period triggers a significant liquid movement along the very permeable longitudinal direction which supplied the end-piece in liquid [76]. The length is the distance from the endpiece, MC in dry basis, Temperature in °C and pressure is in bars.

formulation [115, 79, 116, 12].

Nowadays, even more efficient methods are used, for example, either exponential integrators or via temporal discretization using first and second-order, variable-stepsizes backward differentiation formulae [16, 14]. These methods produce a large nonlinear system of equations that must be solved at each time step to advance the solution time. Both solution methodologies use efficient Krylov subspace methods [97] to deal with the large, sparse matrix systems that result from the spatial discretization. In the former, the challenge is to approximate the action of a matrix function involving the so-called  $\varphi$ -function defined as  $\varphi(z) = \frac{\exp(z)-1}{z}$  on a vector, while in the later a right-preconditioned GMRES iterative solver is used to compute the solution of the linearized Newton system in a globally convergent, Jacobian-free Newton-Krylov framework.

## 5. The contribution of modeling in parameter characterization

One has to emphasize that the macroscopic formulation discussed throughout the previous section required a long list of material parameters to be supplied to the model as input parameters. In addition, most of these parameters are dependent on temperature and even more strongly dependent on moisture content. This is the case, for example, for capillary pressure and the liquid and gas phase relative permeabilities [20]. This need is one of the major issues faced for a drying simulation : applying an existing code to a

325 new product requires an extensive characterization of the new material to be performed  
to determine the relevant parameters.

To address this issue, the computational solution of the macroscopic formulation is, nowa-  
days, a fantastic tool to guide the experimentation. With a full solution in less than one  
330 second, the code can be used as a physical engine in an inverse procedure to identify a  
particular product parameter [72, 93]. This allows the tedious experimental characteriza-  
tion to be considerably simplified. As the computational tool allows the actual conditions  
applied to the sample to be taken into consideration, it is no longer necessary to have a  
perfect control of the experiment, it is only the actual conditions and their effect on the  
335 sample that need to be registered.

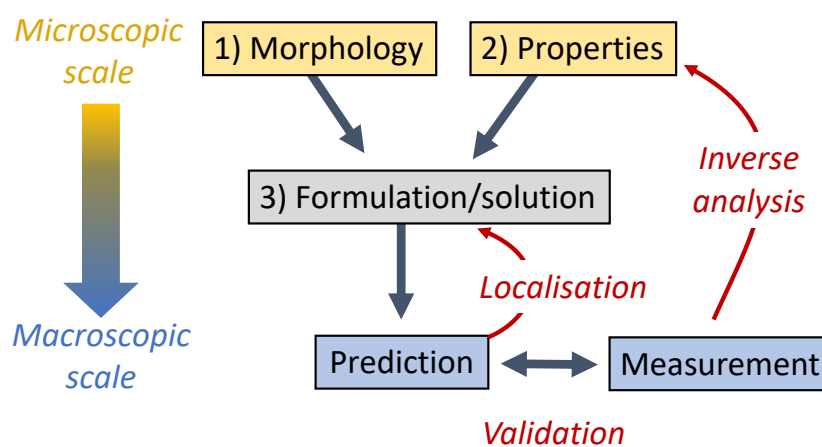


Figure 5: The principle of upscaling to predict the macroscopic properties of an heterogeneous medium from the properties of the phases and their properties.

It is worth noting that the latest developments in materials science allow computational  
science to achieve what was just a dream a few decades ago. When scientists proposed the  
method of volume averaging [105, 26, 47] or the homogenization theory [10, 100, 2], their  
340 goal was just to provide a rigorous pathway for a change of scale and derive the equivalent  
macroscopic equations. For some time, the use of computational homogenization tech-  
niques was limited to simple virtual unit cells, even when intended to approximate real  
morphologies [10, 78]. Nowadays, the progress in this field is spectacular, both in terms  
of the computing power and in 3D imaging capability [74, 57]. It is therefore possible  
345 to propose a completely virtual approach of materials, the so-called concept of digital  
twin in materials science. Whatever the upscaling method (volume averaging or homog-  
enization), the change of scale needs the morphology of the phases to be defined over  
a representative subset of the material (unit cell or Representative Elementary Volume).  
The local properties of these phases are also part of the input data for upscaling. With  
350 these two pieces of information now readily available to scientists, the upscaling formu-  
lation and its computational solution permit the macroscopic properties of the material  
under investigation to be predicted (Fig. 5).

The chain of tools involved in this process includes high resolution 3D imaging, image-  
based meshing and solving either homogenization or volume averaging on the digital

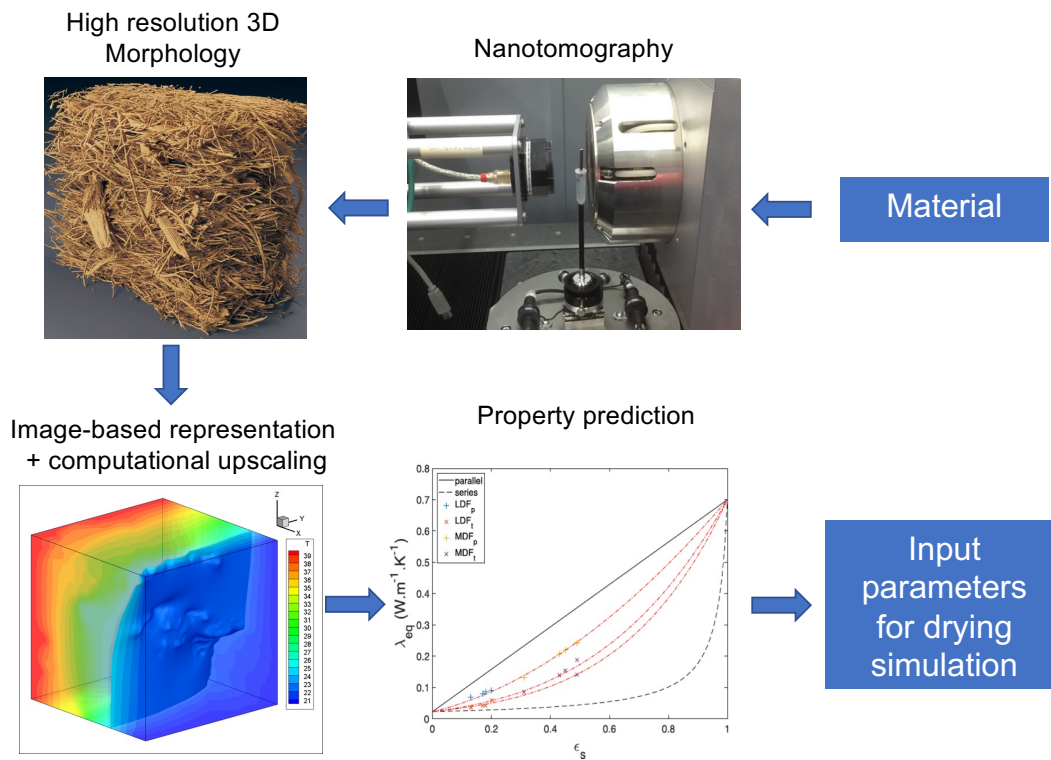


Figure 6: From the product to the prediction of properties by upscaling : the concept of digital twin in materials science [44].

355 representation of the heterogeneous material (Fig. 6). The direct scheme can also be used  
 in an inverse approach, particularly for products of biological origin for which it is very  
 difficult to characterize the local properties. The unknown local property is adjusted for  
 the predicted and measured values at the macroscopic levels to be similar. Once done,  
 the macroscopic properties of a product having the same solid phase, but different mor-  
 360 phologies, can be predicted with accuracy.

Such possibilities open a new field of "virtual" characterization of a material. This is cer-  
 tainly one of the promising routes to render the drying models more operational and more  
 flexible regarding the product of interest. For example, this method has been applied with  
 365 success to predict permeability [85, 24, 1], thermal and mass diffusivity [44, 25, 88] and  
 mechanical properties [127, 40, 43, 5]. It is even possible to tackle complex problems such  
 as the partition of capillary liquid in a real pore morphology [107].

## 6. The mechanical aspects of drying : product deformation and drying stress

During drying, most products exhibit a reduction of size, the shrinkage, resulting from  
 370 water removal. Free shrinkage can be determined using small samples while removing  
 water gently, to ensure a quasi-uniform MC field within the sample. However, in real dry-  
 ing configuration, the local shrinkage, as defined by free shrinkage induced by the local  
 MC value, does not satisfy the compatibility conditions (the strain cannot be integrated

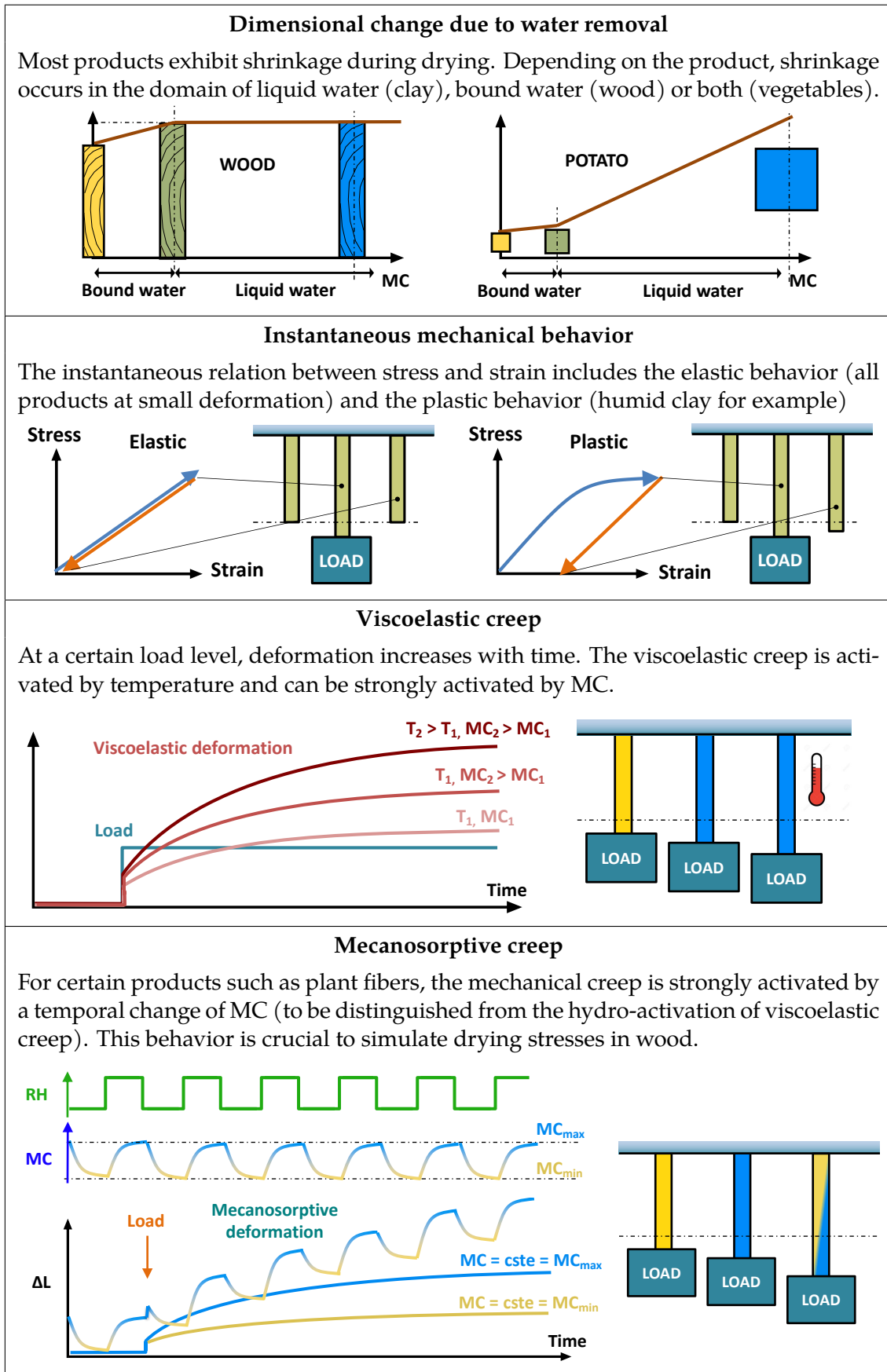
into a displacement field). Consequently, an additional strain field, related to a stress  
375 field, develops for the total field to be compatible. In turn, this stress level produces ad-  
ditional strain tied to the constitutive law of the product : here one talks of, for example,  
viscoelastic creep, mechano-sorptive creep, plastic deformation... These additional strain  
fields act on the drying stresses and a complex process takes place over time. Similarly to  
380 our discussion on coupled transfers, we decided to put the whole formulation of drying  
stresses in annex B and to focus here on the physical interpretation of these phenomena.

Table 2 details all individual behaviors that must be considered to predict the drying  
stresses and their evolution in time. Shrinkage is the primary phenomenon as it is the  
driver for drying stresses. The removal of water usually induces a shrinkage of the solid,  
385 with the exception of inert products such as a bed of sand. However, depending on the  
product, the shrinkage behavior can be very different. For example, wood exhibits shrink-  
age only when bound water is removed : with the exception of species prone to collapse,  
shrinkage occurs only in the hygroscopic domain. Wood is also strongly anisotropic, with  
a total shrinkage ranging from almost zero in the longitudinal direction, to the order of  
390 10% in the tangential direction. In the case of vegetables, the anisotropy is much lower  
and shrinkage occurs mainly in the domain of liquid water, due to a complete collapse  
of the cells. Consequently, reductions in length up to 60%, and 10 fold in volume are ob-  
served [65].

395 Once shrinkage develops at the external zones of a drying product, drying stresses de-  
velop to balance the stress and strain fields. For the rest of the process, drying occurs  
under stress. The mechanical behavior of the solid should therefore be understood and  
considered in the drying model to predict drying stresses. The most important behaviors  
are summarized in Table 2:

- 400 • The simplest behavior is the **linear elasticity** : linearity between stress and strain  
and full recovery once the load is removed. It is important to keep in mind that MC  
might have a significant impact on the stiffness, with an increased stiffness at low  
MC,
- 405 • **Plasticity** refers to a non-linear behavior, but without any effect of time. When the  
load exceeds the elasticity limit, some materials exhibit plasticity : the plastic part of  
strain is not recovered when the load is removed. Humid clay is a perfect example  
of plastic solid,
- 410 • **Viscoelasticity** refers to an increase of strain under load over time. For the products  
considered in drying, thermo- and hydro-activation are of utmost important. The  
characteristic time of viscoelastic creep can be short at high temperature and high  
MC, easily occurring during drying. On the contrary, it can be much longer at low  
MC and moderate temperature, much longer than the drying process, or even longer  
than the lifetime of the product,
- 415 • Finally, it is worth mentioning the existence of an even more complex behavior : the  
**mechano-sorptive creep**. This refers to the activation of the creep (increase of de-  
formation over time) when the solid is submitted to changes of MC under load. This  
is observed for polymers likely to have a large amount of bound water molecules. In

Table 2: The different mechanical mechanisms involved in stress and deformation during the drying of solids.



420 this case, the change of bound water is likely to accelerate the creep due to macro-molecular mobility. This is crucial to model the development of drying stress in wood, especially in the case of oscillating conditions [95, 98].

When shrinkage starts at the beginning of drying, the shrinkage affects the peripheral zones of the product, while the MC at the core is still very close to the initial value. It is then obvious that the shrinkage field does not satisfy the compatibility conditions (Fig. 7, top). The additional strain needed to obtain a compatible field is a tensile field at the surface and, following the global force balance, a compressive field at the core. When the process continues, these stress levels activate the delayed non-instantaneous mechanical behaviors mentioned above. Progressively, creep deformations are added to free shrinkage. Consistently, once the MC is uniform at the end of drying, the total "free" strain depends on the location :

- 430 • At the surface, the shape is the sum of free shrinkage plus the elongation parallel to the surface due to creep. Similarly, a Poisson's effect reduces its size perpendicular to the surface.
- At the edges, shear creep exist as well.
- 435 • At the core, creep due to compressive stress reduces even more the size compared to pure free shrinkage.

This explains the stress reversal (Fig. 7, bottom) : the peripheral zones are now under compression, while the inner parts are in tension. Case-hardening is another mechanical effect likely to amplify this behavior : for many products, the stiffness increases when MC decreases. The creep occurring at the surface at the beginning of drying is some how frozen once the product is dry due to the increase in stiffness. Experimentally, the total strain (shrinkage + creep) can be assessed by relaxing the stress field (cutting the sample into small parts), or partially assessed by relaxing some of the stress field (the cup method in wood drying for example).

445 Over the last decades, the modeling of drying stresses started with the implementation of very basic mechanical behavior (a simple elastic behavior, which is not realistic). The first works considering creep (viscoelastic or plastic) which were able to produce realistic 1-D simulations, were published in the 80s [110, 6, 51]. This approach also became common from the 90s [99, 17, 36, 86, 94]. However, with the increasing power of computers, 2-D simulations, coupled with a comprehensive heat and mass transfer formulation together with a comprehensive constitutive equation for mechanics, were proposed [28, 66, 27]. Clay and wood are the most popular materials that motivated these works, due to the difficulty in avoiding mechanical defaults during drying. Nowadays, 3D modeling has become quite common [29, 23].

455 The discussion to this point explained how the MC field evolution could be used to obtain the local free shrinkage and, together with a suitable mechanical behavior, is applicable for simulating drying stresses and deformation. However, even though this approach accumulates many difficulties, this is "just" a one-way coupling (8). While this is justified in the case of small strain and small deformations, depending on the geometry, even small strain can produce large deformations. This imposes a suitable mechanical formulation

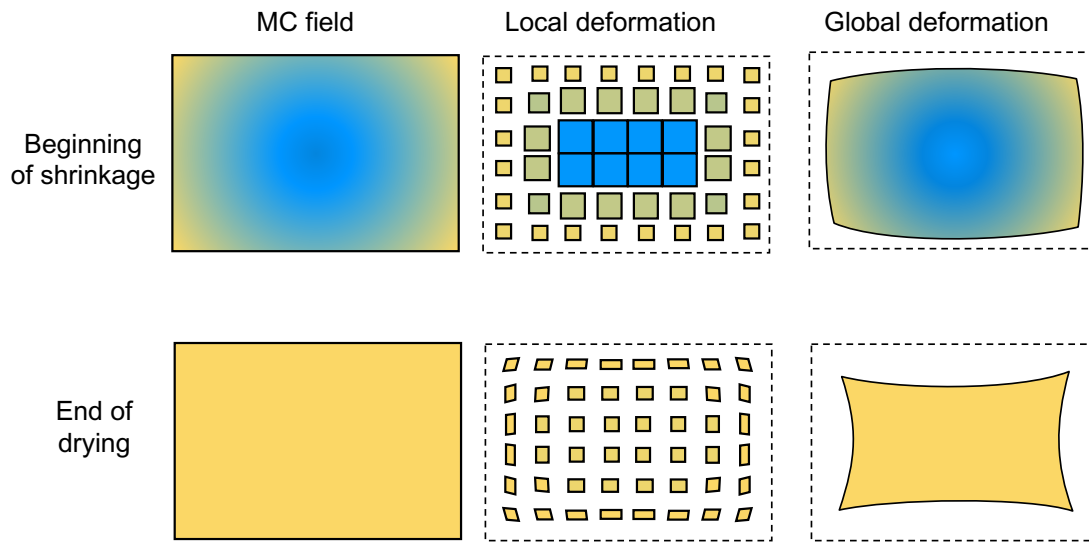


Figure 7: The coupling between stress and deformation during drying, as driven by the shrinkage due to water removal and the effect of mechanical behavior triggered by the drying stresses.

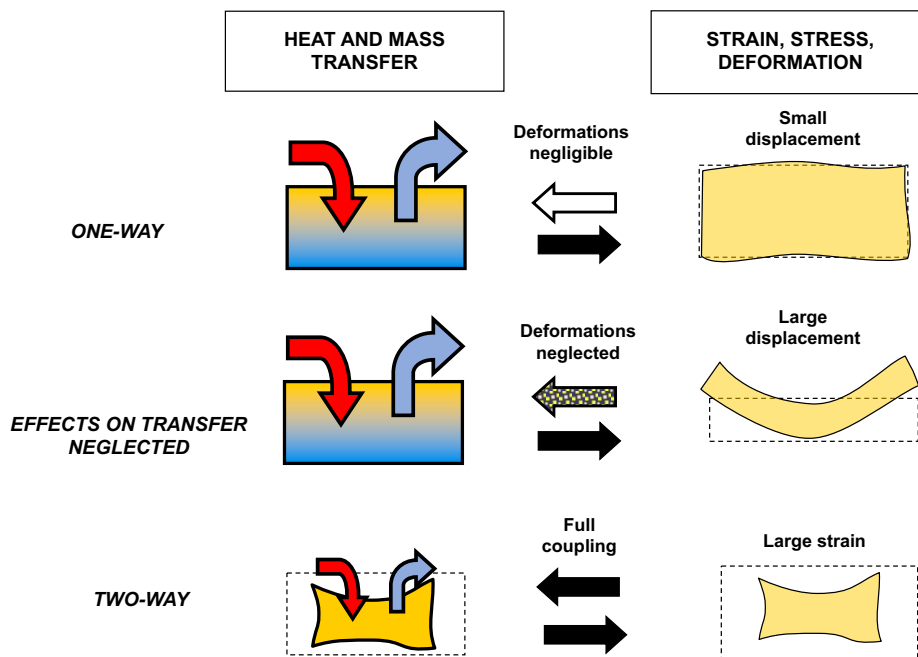


Figure 8: Coupling between transfers and mechanics occurring in drying : the increasing complexity, from a simple one-way coupling to a full coupling.

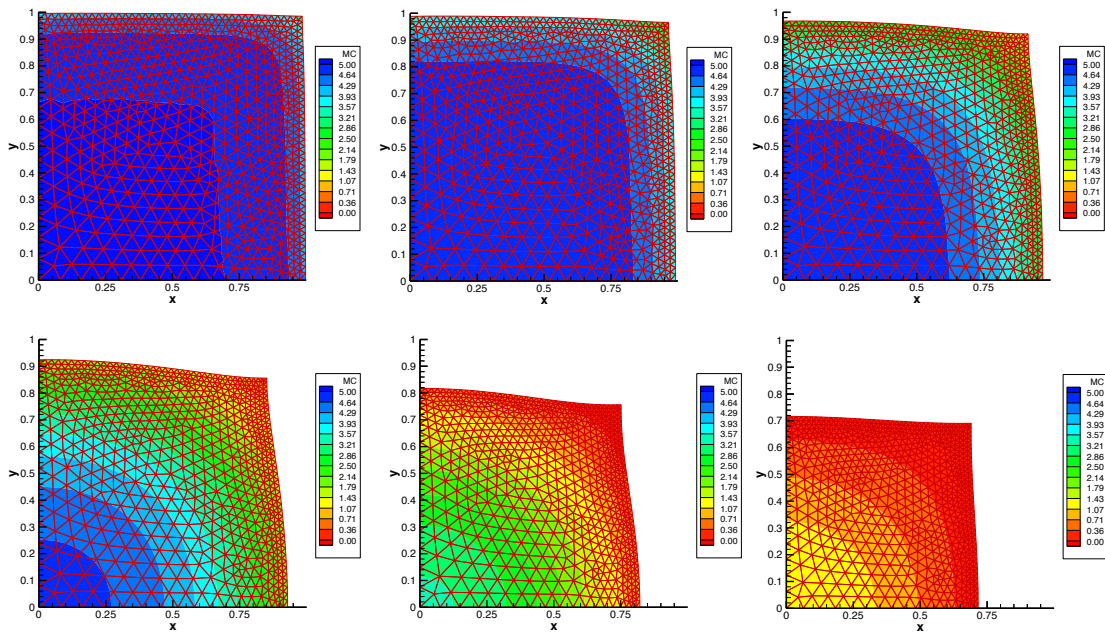


Figure 9: Convective drying of a potato chip during convective drying : dry bulb =  $50^{\circ}\text{C}$ , dew point =  $30^{\circ}\text{C}$ , heat transfer coefficient =  $14 \text{ W}\cdot\text{m}^{-2}\cdot\text{s}^{-1}$ , mass diffusivity =  $3.10^{-10} \text{ m}^2\cdot\text{s}^{-1}$ . Shape and moisture content fields at 1, 2, 5, 10, 20 and 30 hours of drying [64].

to be used (in short, the linear tangent application must be split as a product of rotation and pure deformation), but the effect of deformation on transfer could still be neglected. Finally, in the case of large strain, such as the considerable shrinkage of vegetables, a two-way coupling is mandatory. The change of dimension impacts the MC gradient and must be accounted for in the diffusive fluxes [53]. Similarly, the reduction of exchange surface area reduces the global drying rate, even though the product remains in the constant drying rate (flux) period. Figure 9 depicts simulation results of a two-way coupling model using a large strain and large displacement formulation.

470

The ultimate complexity of the two-way coupling arises when the strain field acts on the MC flux by adding an additional driving force, a local liquid overpressure due to the reduction of solid volume [119].

## 7. Non-local equilibrium

475

In the case of coupled transfer, it is not so rare to observe non-Fickian behavior. This is revealed, for example, by a slow shift in moisture content during a relative humidity (RH) plateau after a sudden change [42], or by a dependence of the mass diffusion coefficient with the sample thickness [91, 82].

480

In products of biological origin, this abnormal behavior is attributed to two phenomena arising at different spatial scales: a non-uniform MC field at the solid phase level (non-local 1 in Fig. 10) and relaxation at the macromolecular scale (non-local 2 in Fig. 10):

- **Dual-scale effects** are likely to occur in heterogeneous materials structured as a connected conductive phase surrounding a storage phase. This can occur in natural

485 products (fractured stones, tissues in biological products [96]), or in manufactured  
products (fiberboard, packed beds). Depending on the sample size and imposed  
conditions, this microstructure may produce local equilibrium failures [37, 59, 77,  
62, 73], which implies that the microscopic fields in the solid phase are nonuniform,

490 • **Molecular relaxation** in polymers has been reported more than six decades ago  
[21]. Re-arrangement at the macromolecular state when a penetrant diffuses into a  
polymer substance requires considerable time, depending on the macromolecular  
mobility. Such effects exist in biomacromolecules [18, 121].

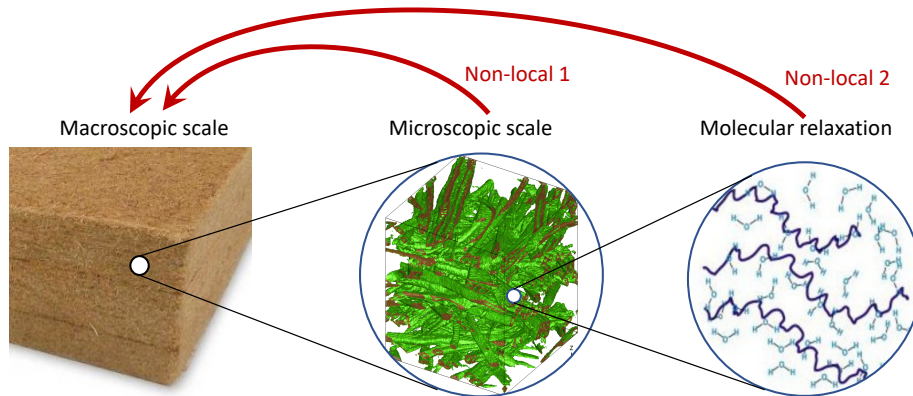


Figure 10: In lignocellulosic materials and biological products, memory effects during transient hydric changes arise from non-uniform field in the solid phase and from molecular relaxation.

The classical formulation of coupled heat and mass transfer therefore cannot represent the experimental facts. The best way to address this problem is to shift from the one-  
495 way connection between scales proposed in the up-scaling method, to a complex two-way coupling between the microscopic and macroscopic scales. In this approach, the microscopic fields in the micro-morphology (the unit cell, representative of product morphology) must be solved and updated over time at each point of the macroscopic mesh [13]. This two-way coupling must be treated at each macroscopic point between the macro-  
500 variables:

- The macroscopic values acts as boundary values at the unit cell level to compute the micro-fields,
- The solutions at the unit cell level provide sink/source terms for the macroscopic balances

505 Figure 11 depicts the results of such dual-scale simulations in the case of fiberboard [75]. Two different thicknesses (1 mm and 20 mm of half-thickness) were selected for the same value of microscopic diffusivity ( $1 \cdot 10^{-13} m^2 \cdot s^{-1}$ ). For each plot, macroscopic profiles are plotted at selected times (MC on the y-axis versus position on the x-axis, with the exchange face at  $x = 0$ ). The moisture content (MC) field inside the microscopic fiber is plotted as colored isovalues in a subset of micro-models evenly distributed over the thickness. The scale of this microscopic field (colored legend) is the same as the macroscopic fields, as the initial and equilibrium MC values are the same at both scales:

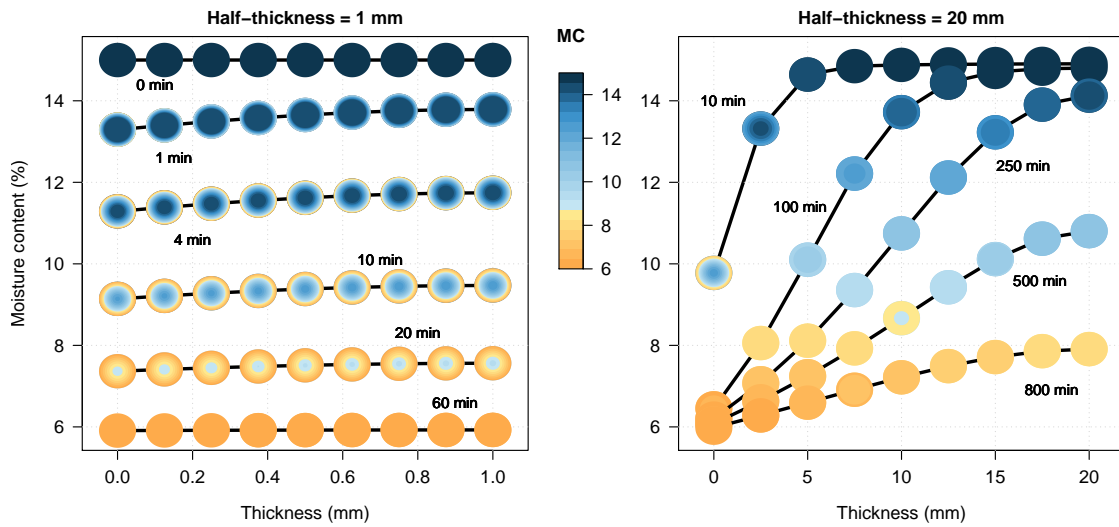


Figure 11: Two contrasted results of the dual-scale model (microscopic mass diffusivity equal to  $10^{-13} m^2 \cdot s^{-1}$ ); left) for two sample thicknesses (left = 1 mm and right = 20 mm). The solid lines represent the macroscopic profiles at selected times, and the colored circles represent the profiles inside a subset of microscopic cells. The exchange surface is at  $x = 0$ .

- For the 1-mm test, the macroscopic profiles remain almost flat, while the microscopic MC fields exhibit significant gradients. In the case of a very thin sample, the behavior is almost entirely controlled by the microscopic diffusion inside the storage phase. The macroscopic resistance to vapor diffusion in the connected pores remains negligible,
- The opposite behavior is observed for the 20-mm thick sample. The resistance to macroscopic diffusion through the conductive phase becomes the dominant effect. Except at the exchange surface and short times, the internal profiles inside the fibers are almost uniform, and classical diffusion profiles develop along the macroscopic thickness.

This dual-scale approach is rigorous and allows many problems to be simulated, such as the drying of packed-beds. This approach is however very demanding in terms of the CPU time. Recently, a general and robust framework was proposed to include non-local equilibrium in the macroscopic formulation of coupled heat and mass transfer [75]. This framework, which was validated using a dual-scale simulation, allows all non-equilibrium effects to be transferred in a macroscopic formulation using a convolution involving memory functions (the two arrows of figure 10) [3, 82].

## 8. Choice of the relevant formulation and number of space variables

This paper presented the state-of-the-art of the physical and mechanical formulation able to provide predictive simulations of the drying process. Among the numerous modeling approaches developed to simulate drying [120], we focused on the class of mechanistic models that are founded on a set of conservation laws which embed all of the necessary physical and mechanical phenomena to ensure they have a high predictive capability.

Once calibrated using experimental data, these models are able to predict situations that were not experimentally calibrated previously. This is a great advantage compared to the simplified modeling approaches used to represent known situations, such as the concept of the characteristic drying curve [118]. Our choice of continuous formulations excludes  
 540 also discrete approaches, for example those based on the use of pore networks [41, 109]. The latter can be categorized as knowledge models that are used for studying the effect of emerging behaviors, but are not intended to be directly applicable at the scale of the drying operation.

545 However, we have to keep in mind that the spatio-temporal formulations presented in the previous section remains complex to implement. This, together with the large number of characterization parameters needed in the model, continues to motivate many scientists to reduce the complexity, either by simplifying the comprehensive macroscopic formulation, or by limiting the number of the spatial dimensions retained in the simulations.

550 Reducing the formulation depends on the choice of the number of independent variables:

- A three-variable model : the comprehensive formulation as described in the previous section, which allows the fields of temperature, moisture content and total gaseous pressure to be updated in time,
- 555 • A two-variable model : by removing the balance of the gaseous phase under the assumption of constant pressure, two balance equations are retained (enthalpy and moisture), which permits the field of temperature and MC to be computed. This formulation is no longer capable of simulating high-temperature configurations, but still takes into consideration the coupling between heat and mass transfer, which is  
 560 one of the key aspects of drying.
- A one-variable model also discards the enthalpy balance. This approach just allows the field of MC to be computed. As an important consequence, the coupled transfers in the boundary layer can only be considered in a very simplistic manner, which considerably reduces its predictability [63]. The physics embedded in such a simple  
 565 model is very poor and, basically, should NOT be used nowadays, except in the rare case where the coupling is negligible.

A dimensionless number, the Drying Intensity Number, was introduced in Perré [63] to quantify the level of heat and mass transfer coupling. This dimensionless number was constructed as a ratio of characteristic times:

- 570 • The time constant  $\tau_{int}$  tied to internal mass transfer, simply obtained as the time constant of a diffusion process, using a representative value of mass diffusivity; and
- the time constant  $\tau_{ext}$  tied to the external conditions, evaluated as the time required to remove the total moisture of the product, assuming the drying flux to be that of the CDR period.

575 The Drying Intensity Number, defined as the ratio of these two time constants, reads as:

$$N_{DI} = \frac{\tau_{int}}{\tau_{ext}} = \frac{\ell h \Delta T}{D \rho_s \Delta X L_v}, \quad (3)$$

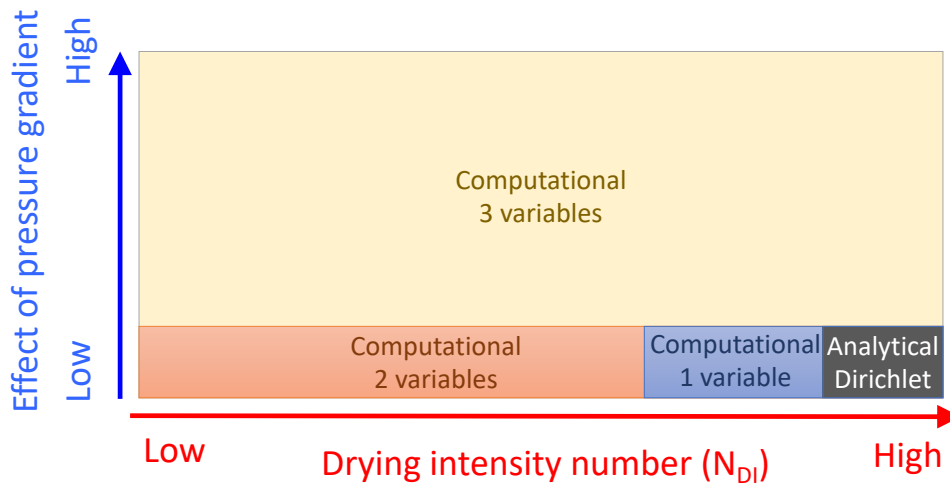


Figure 12: The choice of formulation complexity as a function of drying intensity number and presence of a pressure gradient. The simple analytic solution with boundary conditions is very limited. Regarding the possibilities offered by a computational solution, the predictive capability of the model strongly depends on the number of independent variables and choice of corresponding balance equations.

where  $\ell$  is the characteristic thickness,  $h$  the heat transfer coefficient,  $\Delta T$  the difference between the dry and wet bulb temperatures,  $D$  is a representative value of mass diffusivity,  $\Delta X$  is the change of moisture content, and  $L_v$  the latent heat of evaporation.

580 Accordingly, a high value of  $N_{DI}$  means that the resistance to internal mass transfer governs the drying process. Using two axes ( $N_{DI}$  and effect of gaseous pressure gradient), we can propose recommendations of the suitable formulation to be used as a function of the configuration (Fig.12). The third variable (air balance) is always required when the gradient of total pressure acts on the heat and mass transfer. At the opposite end of the spectrum, a one-variable model could be used only when the whole process is controlled by internal mass transfer (high  $N_{DI}$  values). The use of an analytical solution, namely the simple solution assuming Dirichlet conditions at the interface, is even more restrictive : it not only assumes the resistance to external transfer is negligible, but it assumes the mass diffusivity is constant over the entire range of MC, which is a very strong assumption.

590 Further detail regarding the significance of the Drying Intensity Number using several comprehensive simulations can be found in [63].

To couple the choice of independent variables with the number of space dimensions, a summary is proposed here as a guideline for the reader to identify the best combination, that aligns with the considered configuration and usage of the model (Table 3).

595

Table 3 refers to the classical, comprehensive formulation of coupled heat and mass trans-  
fer in porous media, that should be considered first. In this model, all balance equations  
arise at the same spatial scale and it is assumed that local equilibrium applies. Here,  
600 the effective macroscopic parameters needed to simulate the process can either be ob-  
tained by experimental characterization, or by up-scaling (arrow 1 in figure 13). The  
3-variable model is comprehensive and allows a wide range of configurations to be simu-

Table 3: A simplified guideline to choosing the best compromise between modeling effort and simulation capabilities.

|    | Number of variables   |  |   |
|----|---|--|---|
|    | One (MC)  | Two (MC, T)  | Three (MC, T, P)  |
| 1D | Poor physics, no heat and mass transfer coupling, to be avoided, except when internal mass transfer clearly dominates.                                    | Coupling at low temperature and fast simulation : good choice for obtaining an operational model, for example in parameter identification.               | The 3-variable model is required for "high temperature" configurations, but multidimensional transfers generally occur due to the pressure gradient.            |
| 2D | There is no need to increase the spatial description for such poor physics. It might be of interest for computing drying stresses at high $N_{DI}$ values | Coupling at low temperature and reasonable CPU time : of interest for studying the effect of product geometry.   | Needed for "high temperature" configurations when product geometry is important, and particularly useful for anisotropic media.                                 |
| 3D | There is no need to increase the spatial description for such poor physics. It might be of interest for computing drying stresses at high $N_{DI}$ values | Coupling at low temperature, full 3D description but significant CPU time. Recommended when geometry really matters (complex shapes, drying stresses...) | Needed for "high temperature" configurations when product geometry is important, particularly for anisotropic media when MC is used to compute drying stresses. |

lated, namely any "high temperature" configuration which gives rise to a gradient of the total pressure inside the medium. In the case of "low temperature" configurations, this model can be simplified to the 2-variable case which still accounts for the heat and mass transfer coupling [63]. As recommended in table 3, the one-variable formulation, which discarded the fundamental coupling between heat and mass transfer, should not be used.

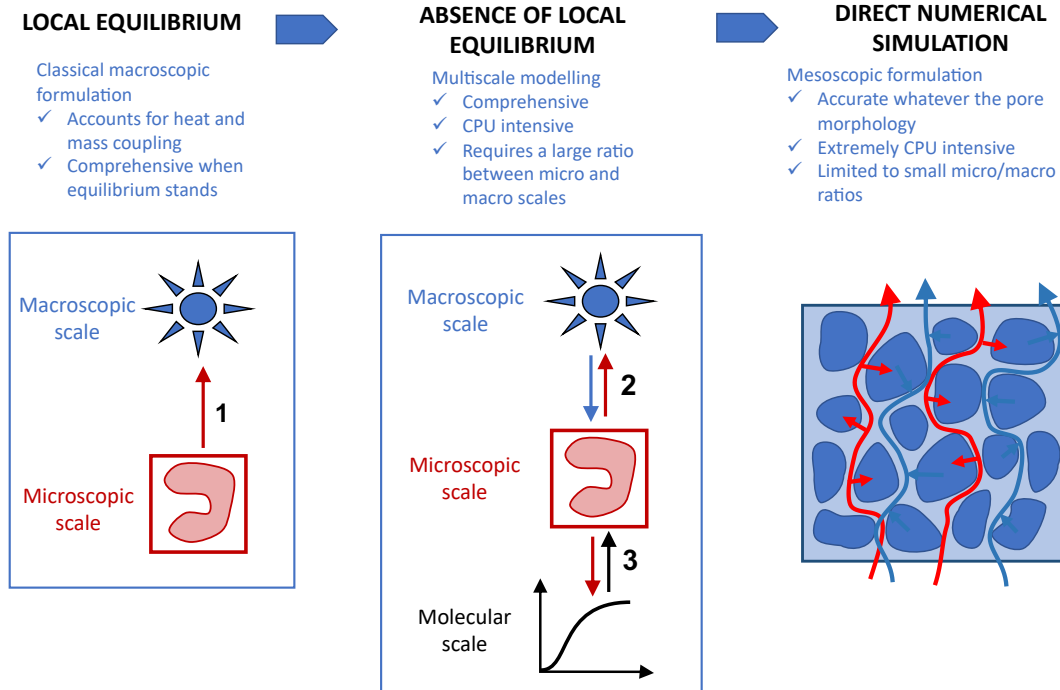


Figure 13: When local equilibrium is not guaranteed, the classical formulation of coupled heat and mass transfer fails. A full multi-scale modeling approach is needed to account for non-local equilibrium and molecular relaxation. A new macroscopic formulation proposed in [75] allows these phenomena to be transferred at the macroscopic scale at a much reduced computational cost.

Even though the comprehensive macroscopic formulation has a wide range of potential applications, it also has some limitations, which are pointed out in the *Non-local equilibrium* section. The failure of local equilibrium is not so obvious to identify [117]. A simple rule consists in comparing the characteristic time constants involved in the problem: time constants of macroscopic phenomena (thermal conduction, mass diffusion, bulk flow related to Darcy's law...), similar phenomena involved at the microscopic scale (transfer in fractured rocks, bound water diffusion in fibers, thermal diffusion in inclusions...) and specific phenomena such as molecular relaxation in polymers. The macroscopic phenomena depends on the product size (typically as the squared size for diffusive phenomena) while the others depend solely on the porous medium morphology and its composition. The assumption of local equilibrium requires that all macroscopic time constants be much larger than all other time constants.

In the case of failure of local equilibrium, a full dual-scale or multi-scale model is needed, i.e. a two-way coupling between the microscopic and the macroscopic scales must be used [103, 30, 83, 73, 90]. This kind of approach is indicated by arrows 2 and 3 in figure 13),

625 however it is very demanding in terms of CPU time [13]. Instead, the multi-scale effects can be efficiently embedded in a macroscopic formulation with memory functions [75]. The usage of such functions, however, assumes the "slow" phase to have a negligible effect in the macroscopic fluxes.

630 Finally, a direct numerical simulation can be proposed thanks to the impressive power of today's computers (Fig. 13, right). In this case, any kind of coupling between scales and any geometry can be considered [22, 15, 58].

## 9. Trends and future prospects of mechanistic drying models

### 9.1. Needs and concerns

635 Drying is by far the most commonly encountered and energy-intensive unit operation in almost all industrial sectors [55]. The urgent need to lower  $CO_2$  emissions in the industry will deeply affect the drying operation : energy issues will certainly become a priority [54, 39]. Energy saving, product saving through drying quality, new processes, use of intermittent energy, use of low-temperature fatal energy, drying conditions adapted to the real time energy cost will have to be used simultaneously to achieve this objective. In this sense, the comprehensive formulation detailed in this review paper is a very powerful tool. In particular, it relies on conservation equations that are founded on physical expressions of all fluxes. Hence, this formulation is predictive in the sense that it is able to predict situations that were not tested previously. For example, all aspects of drying (product quality, drying time, energy consumption...) depend on the whole process. It is therefore impossible to propose a multi-objective optimization without a predictive model able to account for the real time availability of energy, availability in quantity, cost and temperature level.

To solve these coupled and non-linear equations, especially in the cases of multi-scale modeling, is quite demanding in terms of the necessary background skills required in applied and computational mathematics, but it became a standard nowadays. With the impressive power of computers, high performance computing systems, and also desktop personal computers, such drying models should have become a tool readily available to drying practitioners. Yet, this is not what is observed in the drying community. For example, at the International Drying Conferences, the biannual meeting of the international community, it can be confirmed that much simpler models (pure diffusion models, one-variable formulations, analytical solutions...) are still commonly used. Models that do not simulate the evolution of the internal fields, such as the characteristic drying curve proposed by van Meel six decades ago, also remain widely used. Yet, models able to predict situations that were not tested previously need to be spread in the industry to address the current challenges. This is mandatory to investigate new situations such as innovative processes, or the control of standard processes, but with intermittent energy, or time-dependent energy costs.

665 There are three main reasons for this limited dissemination of mechanistic models:

1. Several aspects are still to be included in the present state of the art of mechanistic modeling,

- 670 2. Secondly, one must emphasize an important drawback of the full formulation: it requires many input parameters before the model can be used to simulate the behavior of a given product [122]. This is a very tedious requirement for unknown products,
3. The third reason is probably the lack of standard software, efficient in terms of computational solution, flexible enough to be used by drying practitioners, and, if possible, available as open source.

### 675 9.2. Model improvements

As stated in point 1, some aspects still need to be included in the formulation to address particular situations. For instance, the complexity of biological materials should be better understood and coupled into existing formulations. Evidences point at least three aspects to be considered.

- 680 • The first aspect, although described in the literature, still needs better description: **the role of microstructure** in heat and mass transfer, as well as drying stress and deformation. For example, local biological structures, such as the xylem vessels or the tissue heterogeneities, have a great role in water transport [69, 96, 81]. Moreover, the orientation of these structures into the product defines the product shape and shrinkage after drying [96, 48]. This is not limited to biological products and future developments need to consider more complex structures and account their impact on the model formulation. Multiscale modeling (from the microscopic or even from the molecular scale to macroscopic scale) coupled with modern 3D imaging tools are likely to address these needs [112, 57, 81].
- 685
- 690 • As depicted in figure 1, the optimization of the drying process involved many effects. The ultimate goal of drying modeling is to account for all these effects **at the industrial scale**. To achieve this, a multiscale approach is required, but in this case, we talked of a multiscale expansion towards larger scales : simulation of a whole set of products (packed-bed, stack of boards, stirred particles...), simulation of the dryer behavior (heating power, insulation, spatial variations of drying conditions...). This would allow a comprehensive description of the process, including the product variability and the field of drying conditions inside the dryer. The ultimate goal is to obtain a model that is close enough to the real process to enable multi-objective optimization [67, 80, 22, 46].
- 695
- 700 • The third aspect is related to **the metabolism of living biological materials** and its possible impact on drying. For example, grains with distinct metabolic levels are differently affected by process conditions and technologies, possibly affecting the interaction with water – as demonstrated in the ultrasound-assisted hydration of beans [52]. Future studies are needed to understand the effect of metabolic activity on transport phenomena (bio-active transfers), and how to incorporate it in model formulation.
- 705

### 9.3. The digital twin at the crossroads of mechanistic modeling and data science

The remedy for the second reason probably lies in the fast-growing field of data science. Over the past decade, machine learning (ML) has spread across many areas of engineering science. Autonomous cars and weather forecasting without solving the equations of

710

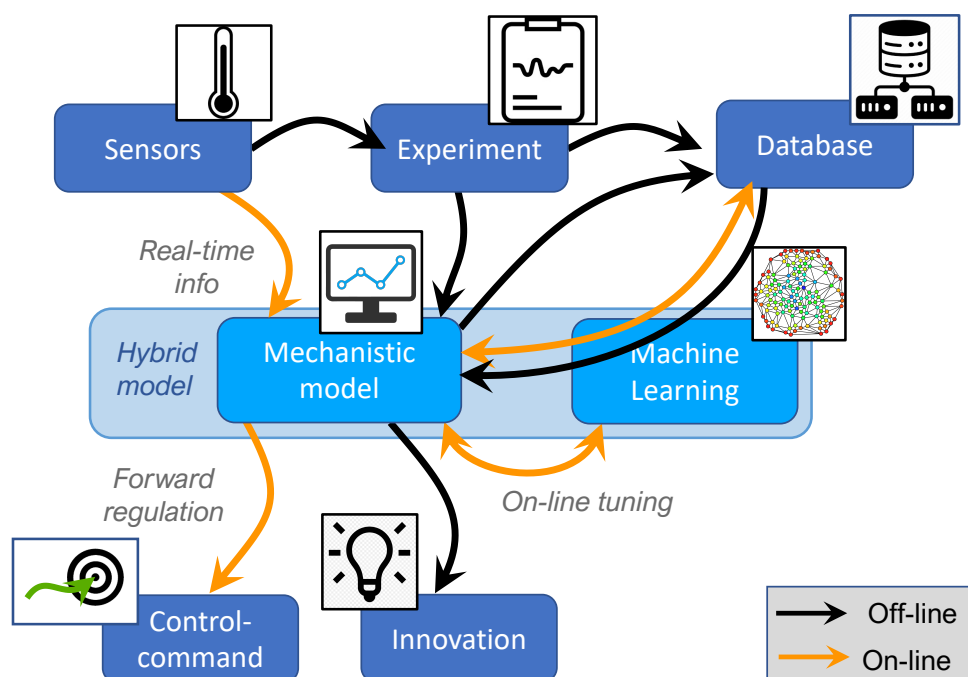


Figure 14: The concept of hybrid modeling : using the synergies between experimentation, mechanistic modeling, data science, and machine learning to fill the gap between modeling and process optimization (control-command and innovation) by the concept of digital twin.

physics are probably the two most popular examples of the success of machine learning. Clearly, ML has also spread to the drying field [108, 50, 35, 34]. However, in most of the works referred to in these review papers, ML is used instead of mechanistic modeling. In this sense, ML is capable of coping with complex situations, provided that the training database is large enough to cover the situations of interest. The predictive capability is restricted to the domain paved by the database.

Rather than using ML instead of mechanistic modeling, we believe that both areas are now mature enough to benefit from the best of both worlds: a predictive model capable of adapting to different products. Such a digital twin approach would work both offline or online [125]. In this hybrid approach, the mechanistic model would remain at the heart of the interactions (Fig. 14).

The off-line work (black arrows in figure 14) includes experimentation, at first devoted to characterizing product parameters, directly supplied to the model as usual, but also to populate a database for later use. This database, together with ML, for example using the graph theory, is able to test the model, and either to reduce it if relevant or, alternatively, to recommend improvement in the formulation (number of variable/space dimensions to consider). The interaction between the model and the database often relies on inverse analyses to determine important parameters, such as relative permeability. Once calibrated, the model itself can be used to complete the database through complex sim-

ulations (for example full 3D simulation to be used later in real-time). As the heart of the system is a mechanistic model, the calibrated model can be used to test and optimize innovative drying processes.

735

The on-line use of the model (orange arrows of figure 14) includes at first the classical approach : using the real-time information gathered by sensors for control/command. As the model is predictive, it is capable of forward regulation, a major advantage for drying, a process for which the final quality/cost depends on the entire history of the process.

740

As the drying of solids is quite slow, ML could be used in this real-time loop to tune the model parameters throughout the process as a function of what is observed. This is a crucial advantage for all processes dealing with biological, hence variable, products. As a last step of complexity, the mechanistic model and the database can work in synergy, as a hybrid approach, in which information provided by the mechanistic model can benefit from the database, with requests triggered and analyzed by ML, to complement the model. It is a way, for example, of using simulations that are impossible to carry out in real time, or for comparing previous situations in order to detect specific issues (technical problems, sensor failure, product anomaly, etc.).

745

#### 750 9.4. Availability of efficient software in the industry

Note that the previous projection needs also to address the third reason for the limited dissemination of mechanistic drying models. The availability of predictive drying models in open-source or commercial software platforms would ease the implementation of these complex models for non-specialists. The co-authors of this review article are highly motivated by the future prospects of these innovative modelling strategies. They are aware that they must play a major role in the development and availability of simulation codes for the drying community.

755

## 10. Conclusion

This review paper presents in a didactic way the state of the art of drying modeling of solids. Numerous illustrations are proposed to facilitate the understanding of all the concepts necessary to elaborate a predictive spatio-temporal formulation of the phenomena involved in a drying solid. At first the coupled heat and mass transfers, but also the complex problem of the mechanical behavior. With an appropriate computational solution and a complete set of parameters, this formulation is able to simulate the drying process in a predictive way. It can then be used to understand the process, to optimize the drying conditions, as a physical driver in an inverse analysis for product characterization, in control/command... The non-local equilibrium is also introduced as one of the limits of the macroscopic formulation.

760

765

To summarize all these concepts, a guide is proposed to help the reader to choose the right level of approach in terms of the number of independent variables and space dimensions. Finally, open questions and the fantastic potential of combining mechanistic modeling and machine learning are outlined.

770

## Acknowledgments

775 The authors would like to thank the Département de la Marne, Grand Reims, Région Grand Est and the European Union along with the European Regional Development Fund (ERDF Champagne Ardenne 2014-2020) for their financial support of the Chair of Biotechnology of CentraleSupélec.

## References

- 780 [1] MA Ali, R Umer, KA Khan, and WJ Cantwell. Application of x-ray computed tomography for the virtual permeability prediction of fiber reinforcements for liquid composite molding processes: A review. *Composites Science and Technology*, 184:107828, 2019.
- [2] Grégoire Allaire. Homogenization and two-scale convergence. *SIAM Journal on Mathematical Analysis*, 23(6):1482–1518, 1992.
- 785 [3] Giana Almeida, Sandra Domenek, and Patrick Perre. Transpoly: A theoretical model to quantify the dynamics of water transfer through nanostructured polymer films. *Polymer*, 191:122256, 2020.
- [4] Javier R Arballo, Laura A Campañone, and Rodolfo H Mascheroni. Modeling of microwave drying of fruits. *Drying Technology*, 28(10):1178–1184, 2010.
- 790 [5] M Assad-Bustillos, S Guessasma, AL Réguerre, and G Della Valle. Impact of protein reinforcement on the deformation of soft cereal foods under chewing conditions studied by x-ray tomography and finite element modelling. *Journal of Food Engineering*, 286:110108, 2020.
- [6] Zdeněk P Bažant. Mathematical model for creep and thermal shrinkage of concrete at high temperature. *Nuclear engineering and Design*, 76(2):183–191, 1983.
- 795 [7] J. Bear and Corapcioglu. *Advances in Transport Phenomena in Porous Media*. Martinus Nijhoff Publishers, Lancaster, 1987.
- [8] R. B. Bird, W. E. Stewart, and E. N. Lightfoot. *Transport Phenomena*. John Wiley & Sons, New York, 1960.
- 800 [9] A Bouali, R Rémond, G Almeida, and P Perré. Thermo-diffusion in wood: X-ray mc profiles analysed using a 2-d computational model. In *Proceedings of the 18th International Drying Symposium*, page 5, 2012.
- [10] Jean-François Bourgat. Numerical experiments of the homogenization method. In *Computing methods in applied sciences and engineering, 1977, I*, pages 330–356. Springer, 1979.
- 805 [11] George Bramhall. Mathematical model for lumber drying. i. principles involved. *Wood science*, 12:14–21, 1979.
- [12] Michaël Bucki and Patrick Perré. Physical formulation and numerical modeling of high frequency heating of wood. *Drying Technology*, 21(7):1151–1172, 2003.
- [13] E. J. Carr, I. W. Turner, and P. Perré. A dual-scale modelling approach for drying hygroscopic porous media. *SIAM Multiscale Modeling and Simulation*, 11:362–384, 2013.
- 810 [14] E. J. Carr, I. W. Turner, and P. Perré. A variable-stepsize jacobian-free exponential integrator for simulating transport in heterogeneous porous media: Application to wood drying. *Journal of Computational Physics*, 233:66–82, 2013.
- [15] E. J. Carr, P. Perré, and I. W. Turner. The extended distributed microstructure model for gradient-driven transport: A two-scale model for bypassing effective parameters. *Journal of Computational Physics*, 327:810–829, 2016.
- 815 [16] Elliot J Carr, Timothy J Moroney, and Ian W Turner. Efficient simulation of unsaturated flow using exponential time integration. *Applied mathematics and computation*, 217(14):6587–6596, 2011.
- 820 [17] Guangnan Chen, RB Keey, and JCF Walker. The drying stress and check development on high-temperature kiln seasoning of sapwoodpinus radiata boards. *Holz als Roh-und Werkstoff*, 55(2):59–64, 1997.

- [18] G.N. Christensen. Sorption and Swelling within Wood Cell Walls. *Nature*, 213:782–784, 1967.
- 825 [19] Thiéry Constant, C Moyne, and P Perre. Drying with internal heat generation: Theoretical aspects and application to microwave heating. *AIChE Journal*, 42(2):359–368, 1996.
- [20] Frédéric Couture, W Jomaa, and J-R Puiggali. Relative permeability relations: a key factor for a drying model. *Transport in porous media*, 23(3):303–335, 1996.
- 830 [21] J. Crank. A theoretical investigation of the influence of molecular relaxation and internal stress on diffusion in polymers. *Journal of Polymer Science*, 11(2):151–168, 1953.
- [22] Thijs Defraeye. Advanced computational modelling for drying processes—a review. *Applied Energy*, 131:323–344, 2014.
- [23] Sara Florisson, Johan Vessby, and Sigurdur Ormarsson. A three-dimensional numerical analysis of moisture flow in wood and of the wood’s hygro-mechanical and visco-elastic behaviour. *Wood Science and Technology*, 55(5):1269–1304, 2021.
- 835 [24] Yuan Gao, Xiaoxian Zhang, Pratap Rama, Ying Liu, Rui Chen, Hossein Ostadi, and Kyle Jiang. Calculating the anisotropic permeability of porous media using the lattice boltzmann method and x-ray computed tomography. *Transport in porous media*, 92(2):457–472, 2012.
- 840 [25] Pablo A García-Salaberri, Iryna V Zenyuk, Andrew D Shum, Gisuk Hwang, Marcos Vera, Adam Z Weber, and Jeff T Gostick. Analysis of representative elementary volume and through-plane regional characteristics of carbon-fiber papers: diffusivity, permeability and electrical/thermal conductivity. *International Journal of Heat and Mass Transfer*, 127:687–703, 2018.
- [26] W.G. Gray. A derivation of the equations for multiphase transport. *Chemical Engineering Science*, 30:229–233, 1975.
- 845 [27] I Hammouda and D Mihoubi. Modelling of drying induced stress of clay: elastic and viscoelastic behaviours. *Mechanics of Time-Dependent Materials*, 18(1):97–111, 2014.
- [28] MN Haque, TAG Langrish, L-B Keep, and RB Keey. Model fitting for visco-elastic creep of pinus radiata during kiln drying. *Wood Science and Technology*, 34(5):447–457, 2000.
- 850 [29] M Heydari, K Khalili, and SY Ahmadi-Brooghani. More comprehensive 3d modeling of clay-like material drying. *AIChE Journal*, 64(4):1469–1478, 2018.
- [30] U. Hornung, editor. *Homogenization and porous media*. Springer-Verlag, New York, 1997.
- [31] M Ilic and IW Turner. Convective drying of a consolidated slab of wet porous material. *International Journal of Heat and Mass Transfer*, 32(12):2351–2362, 1989.
- 855 [32] H Iyota, N Nishimura, M Yoshida, and T Nomura. Simulation of superheated steam drying considering initial steam condensation. *Drying Technology*, 19(7):1425–1440, 2001.
- [33] Can-Chun Jia, Da-Wen Sun, and Chong-Wen Cao. Mathematical simulation of temperature and moisture fields within a grain kernel during drying. *Drying Technology*, 18(6):1305–1325, 2000.
- 860 [34] Md Imran H Khan, Shyam S Sablani, MUH Joardder, and MA Karim. Application of machine learning-based approach in food drying: Opportunities and challenges. *Drying Technology*, 40(6):1051–1067, 2022.
- [35] Md Imran H Khan, Shyam S Sablani, Richi Nayak, and Yuantong Gu. Machine learning-based modeling in food processing applications: State of the art. *Comprehensive Reviews in Food Science and Food Safety*, 21(2):1409–1438, 2022.
- 865 [36] Stefan Jan Kowalski and Kinga Rajewska. Drying-induced stresses in elastic and viscoelastic saturated materials. *Chemical Engineering Science*, 57(18):3883–3892, 2002.
- [37] K. Krabbenhoft and L. Damkilde. Double porosity models for the description of water infiltration in wood. *Wood Science and Technology*, 38:641–659, 2004.
- 870 [38] O Krischer and K Kröll. *Die wissenschaftlichen Grundlagen der Trocknungstechnik*. Springer, Berlin, 1956.
- [39] T Kudra. Energy aspects in drying. *Drying Technology*, 22(5):917–932, 2004.
- [40] Cédric P Laurent, Pierre Latil, Damien Durville, Rachid Rahouadj, Christian Geindreau, Laurent Orgéas, and Jean-François Ganghoffer. Mechanical behaviour of a fibrous scaffold for ligament tissue engineering: Finite elements analysis vs. x-ray tomography imaging.
- 875

- Journal of the mechanical behavior of biomedical materials*, 40:222–233, 2014.
- [41] Y Le Bray and M Prat. Three-dimensional pore network simulation of drying in capillary porous media. *International journal of heat and mass transfer*, 42(22):4207–4224, 1999.
- [42] D. Lelievre, T. Colinart, and P. Glouannec. Hygrothermal behavior of bio-based building materials including hysteresis effects: Experimental and numerical analyses. *Energy and Buildings*, 84:617–627, 2014.
- [43] Yang Liu, Ilya Straumit, Dmytro Vasiukov, Stepan V Lomov, and Stéphane Panier. Prediction of linear and non-linear behavior of 3d woven composite using mesoscopic voxel models reconstructed from x-ray micro-tomography. *Composite structures*, 179:568–579, 2017.
- [44] M. Louërat, M. Ayouz, and P. Perré. Heat and moisture diffusion in spruce and wood panels computed from 3-D morphologies using the Lattice Boltzmann method. *International Journal of Thermal Sciences*, 130:471–483, 2018.
- [45] Alexei Vasilievich Luikov. Heat and mass transfer in capillary-porous bodies. In *Advances in heat transfer*, volume 1, pages 123–184. Elsevier, 1964.
- [46] Martial Madoumier, Gilles Trystram, Patrick Sébastien, and Antoine Collignan. Towards a holistic approach for multi-objective optimization of food processes: a critical review. *Trends in Food Science & Technology*, 86:1–15, 2019.
- [47] C. Marle. On macroscopic equations governing multiphase flow with diffusion and chemical reactions in porous media. *Int. J. Eng. Sci.*, 20:643–662, 1982.
- [48] Bianca Marques, Patrick Perré, Joel Casalinho, Carmen C. Tadini, Artemio Plana-Fattori, and Giana Almeida. Evidence of iso-volume deformation during convective drying of yacón: An extended van Meel model adapted to large volume reduction. *Journal of Food Engineering*, 341:111311, 2023. ISSN 0260-8774. doi: <https://doi.org/10.1016/j.jfoodeng.2022.111311>. URL <https://www.sciencedirect.com/science/article/pii/S026087742200365X>.
- [49] Benoît Martin. *Dynamique des transferts d’humidité au sein de l’épicéa commun (Picea abies (L.) Karst.): mesures par imagerie X et simulations numériques*. PhD thesis, Université de Lorraine, 2022.
- [50] Alex Martynenko and NN Misra. Machine learning in drying. *Drying Technology*, 38(5-6): 596–609, 2020.
- [51] J Kofi Mensah, GL Nelson, MY Hamdy, and TG Richard. A mathematical model for predicting soybean seedcoat cracking during drying. *Transactions of the ASAE*, 28(2):580–0587, 1985.
- [52] Alberto Claudio Miano, Viviane Deroldo Sabadoti, and Pedro Esteves Duarte Augusto. Combining ionizing irradiation and ultrasound technologies: effect on beans hydration and germination. *Journal of food science*, 84(11):3179–3185, 2019.
- [53] D Mihoubi, F Zagrouba, Jean Vaxelaire, A Bellagi, and M Roques. Transfer phenomena during the drying of a shrinkable product: modeling and simulation. *Drying Technology*, 22(1-2):91–109, 2004.
- [54] Arun S Mujumdar. Research and development in drying: Recent trends and future prospects. *Drying Technology*, 22(1-2):1–26, 2004.
- [55] Arun S Mujumdar. *Handbook of Industrial Drying*. CRC Press, 2014.
- [56] S Ben Nasrallah and P Perre. Detailed study of a model of heat and mass transfer during convective drying of porous media. *International journal of heat and mass transfer*, 31(5):957–967, 1988.
- [57] Dang Mao Nguyen, Giana Almeida, Thi Mai Loan Nguyen, Jing Zhang, Pin Lu, Julien Colin, and Patrick Perré. A critical review of current imaging techniques to investigate water transfers in wood and biosourced materials. *Transport in Porous Media*, 137(1):21–61, 2021.
- [58] M. Nouri and P Perré. Direct numerical simulation of coupled heat and mass transfer in hygroscopic porous media. paper 534, 8 pages, IDS’2022, <https://doi.org/10.55900/lavrknht>, 2022.
- [59] U. Nyman, P.J. Gustafsson, B. Johannesson, and R. Hägglund. A numerical method for the evaluation of non-linear transient moisture flow in cellulosic materials. *International Journal*

- for *Numerical Methods in Engineering*, 66:1859–1883, 2006.
- 930 [60] Suhas Patankar. *Numerical heat transfer and fluid flow*. CRC press, 1980.
- [61] Chen Peishi and David CT Pei. A mathematical model of drying processes. *International Journal of heat and mass transfer*, 32(2):297–310, 1989.
- [62] P. Perré. Multiscale aspects of heat and mass transfer during drying. *Transport in Porous Media*, 33:2463–2478, 2007.
- 935 [63] P. Perré. The proper use of mass diffusion equations in drying modeling: Introducing the drying intensity number. *Drying Technology*, 33:1949–1962, 2015.
- [64] P Perré and BK May. A numerical drying model that accounts for the coupling between transfers and solid mechanics. case of highly deformable products. *Drying Technology*, 19(8):1629–1643, 2001.
- 940 [65] P Perré and BK May. The existence of a first drying stage for potato proved by two independent methods. *Journal of food engineering*, 78(4):1134–1140, 2007.
- [66] P Perré and Joëlle Passard. A physical and mechanical model able to predict the stress field in wood over a wide range of drying conditions. *Drying Technology*, 22(1-2):27–44, 2004.
- [67] P. Perré and R. Remond. A dual-scale computational model of kiln wood drying including single board and stack level simulation. *Drying Technology*, 26(9):1069–1074, 2006.
- 945 [68] P. Perré and I. W. Turner. A 3D version of Transpore: a comprehensive heat and mass transfer computational model for simulating the drying of porous media. *International Journal for Heat and Mass Transfer*, 42:4501–4521, 1999.
- [69] P. Perré and I. W. Turner. A heterogeneous wood drying computational model that accounts for material property variation across growth rings. *Chem. Eng. J.*, 86:117–131, 2002.
- 950 [70] P Perré and IW Turner. The use of numerical simulation as a cognitive tool for studying the microwave drying of softwood in an over-sized waveguide. *Wood Science and Technology*, 33(6):445–464, 1999.
- [71] P. Perré, R. Remond, and I. W. Turner. Comprehensive drying models based on volume averaging: Background, application and perspective. In E. Tsotsas and A. S. Mujumdar, editors, *Modern Drying Technology*, volume 1. Wiley-VCH, 2007.
- 955 [72] P. Perré, F. Pierre, J. Casalinho, and M. Ayouz. Determination of the mass diffusion coefficient based on the relative humidity measured at the back face of the sample during unsteady regimes. *Drying Technology*, 33:1068–1075, 2015.
- 960 [73] Patrick Perré. Multiscale modeling of drying as a powerful extension of the macroscopic approach: application to solid wood and biomass processing. *Drying Technology*, 28(8):944–959, 2010.
- [74] Patrick Perré. A review of modern computational and experimental tools relevant to the field of drying. *Drying technology*, 29(13):1529–1541, 2011.
- 965 [75] Patrick Perré. Coupled heat and mass transfer in biosourced porous media without local equilibrium: a macroscopic formulation tailored to computational simulation. *Int. J. Heat Mass Transfer*, 140:717–730, 2019.
- [76] Patrick Perré and A\_ Degiovanni. Simulation par volumes finis des transferts couplés en milieux poreux anisotropes: séchage du bois à basse et à haute température. *International Journal of Heat and Mass Transfer*, 33(11):2463–2478, 1990.
- 970 [77] Patrick Perré and Romain Rémond. A dual-scale computational model of kiln wood drying including single board and stack level simulation. *Drying Technology*, 24(9):1069–1074, 2006.
- [78] Patrick Perré and Ian Turner. Determination of the material property variations across the growth ring of softwood for use in a heterogeneous drying model. part 2. use of homogenisation to predict bound liquid diffusivity and thermal conductivity. *Holzforschung*, 55(4):417–425, 2001.
- 975 [79] Patrick Perre and Ian W Turner. Microwave drying of softwood in an oversized waveguide: Theory and experiment. *AIChE Journal*, 43(10):2579–2595, 1997.
- 980 [80] Patrick Perré, Romain Rémond, Julien Colin, Eric Mougél, and Giana Almeida. Energy consumption in the convective drying of timber analyzed by a multiscale computational model. *Drying Technology*, 30(11-12):1136–1146, 2012.

- [81] Patrick Perré, Dang Mao Nguyen, and Giana Almeida. A macroscopic washburn approach of liquid imbibition in wood derived from x-ray tomography observations. *Scientific reports*, 12(1):1–14, 2022.
- 985 [82] Patrick Perré, Romain Rémond, and Giana Almeida. Multiscale analysis of water vapor diffusion in low density fiberboard: Implications as a building material. *Construction and Building Materials*, 329:127047, 2022.
- [83] M. A. Peter and R. E. Showalter. Homogenization of secondary-flux models of partially fissured media. *International Journal of Numerical Analysis and Modeling*, 5:150–156, 2008.
- 990 [84] JR Philip and DA De Vries. Moisture movement in porous materials under temperature gradients. *Eos, Transactions American Geophysical Union*, 38(2):222–232, 1957.
- [85] Marzio Piller, Gianni Schena, M Nolich, S Favretto, F Radaelli, and E Rossi. Analysis of hydraulic permeability in porous media: from high resolution x-ray tomography to direct numerical simulation. *Transport in porous media*, 80(1):57–78, 2009.
- 995 [86] G Ponsart, J Vasseur, JM Frias, Albert Duquenoy, and Jean-Michel Méot. Modelling of stress due to shrinkage during drying of spaghetti. *Journal of Food Engineering*, 57(3):277–285, 2003.
- [87] J Ri Puiggali, M Quintard, and S Whitaker. Drying granular porous media: gravitational effects in the isenthalpic regime and the role of diffusion models. *Drying Technology*, 6(4):601–629, 1988.
- 1000 [88] El-Houssaine Quenjel and Patrick Perré. Computation of the effective thermal conductivity from 3d real morphologies of wood. *Heat and Mass Transfer*, pages 1–12, 2022.
- [89] M Quintard and JR Puiggali. Numerical modelling of transport processes during the drying of a granular porous medium. *Heat and technology*, 4(2):37–57, 1986.
- [90] Mohammad Mahbubur Rahman, Mohammad UH Joardder, Md Imran Hossen Khan, Nghia Duc Pham, and MA Karim. Multi-scale model of food drying: Current status and challenges. *Critical reviews in food science and nutrition*, 58(5):858–876, 2018.
- 1005 [91] R. Rémond and G. Almeida. Mass diffusivity of low-density fibreboard determined under steady- and unsteady-state conditions : Evidence of dual-scale mechanisms in the diffusion. *Wood Material Science & Engineering*, 6:23–33, 2011.
- 1010 [92] R Rémond and P Perré. High-frequency heating controlled by convective hot air: toward a solution for on-line drying of softwoods. *Drying Technology*, 26(5):530–536, 2008.
- [93] R. Rémond, R. Baettig, and P. Perré. Identification of relative permeability curves for softwood using a computational model and moisture content profiles determined by x-ray absorptiometry. In *15th International Drying Symposium, Drying'2006, Budapest, Hungary*, volume C, pages 1793–1797, 2006.
- 1015 [94] Romain Remond, Joëlle Passard, and Patrick Perré. The effect of temperature and moisture content on the mechanical behaviour of wood: a comprehensive model applied to drying and bending. *European Journal of Mechanics-A/Solids*, 26(3):558–572, 2007.
- [95] Romain Rémond, Mariella De La Cruz, Daniel Aléon, and Patrick Perré. Investigation of oscillating climates for wood drying using the flying wood test and loaded beams: need for a new mechano-sorptive model. *Maderas. Ciencia y tecnología*, 15(3):269–280, 2013.
- 1020 [96] Meliza Lindsay Rojas and Pedro ED Augusto. Microstructure elements affect the mass transfer in foods: The case of convective drying and rehydration of pumpkin. *Lwt*, 93:102–108, 2018.
- 1025 [97] Yousef Saad. *Iterative methods for sparse linear systems*. SIAM, 2003.
- [98] Thouraya Salem, Patrick Perré, Anis Bouali, Eric Mougél, and Romain Rémond. Experimental and numerical investigation of intermittent drying of timber. *Drying Technology*, 35(5):593–605, 2017.
- [99] J-G Salin. Numerical prediction of checking during timber drying and a new mechano-sorptive creep model. *Holz als Roh-und Werkstoff*, 50(5):195–200, 1992.
- 1030 [100] E Sanchez-Palencia. Homogenization method for the study of composite media. In *Asymptotic Analysis II*—, pages 192–214. Springer, 1983.
- [101] Sadoth sandoval Torres, Wahbi Jomaa, Jean-Rodolphe Puiggali, and Stavros Avramidis. Multiphysics modeling of vacuum drying of wood. *Applied Mathematical Modelling*, 35(10):

- 5006–5016, 2011.
- 1035 [102] JR Sharp. A review of low temperature drying simulation models. *Journal of Agricultural Engineering Research*, 27(3):169–190, 1982.
- [103] R. E. Showalter. Distributed microstructured models of porous media. *International Series of Numerical Mathematics*, 114:155–163, 1993.
- 1040 [104] John F Siau and Z Jin. Nonisothermal moisture diffusion experiments analyzed by four alternative equations. *Wood Science and Technology*, 19(2):151–157, 1985.
- [105] J.C. Slattery. *Momentum, Energy and Mass Transfer in Continua*. McGraw-Hill, New York, 1972.
- [106] MA Stanish, GS Schajer, and Ferhan Kayihan. A mathematical model of drying for hygroscopic porous media. *AIChE Journal*, 32(8):1301–1311, 1986.
- 1045 [107] František Štěpánek, Miroslav Šoóš, and Pavol Rajniak. Characterisation of porous media by the virtual capillary condensation method. *Colloids and Surfaces A: Physicochemical and Engineering Aspects*, 300(1-2):11–20, 2007.
- [108] Qing Sun, Min Zhang, and Arun S Mujumdar. Recent developments of artificial intelligence in drying of fresh food: A review. *Critical reviews in food science and nutrition*, 59(14):2258–2275, 2019.
- 1050 [109] VK Surasani, T Metzger, and E Tsotsas. A non-isothermal pore network drying model with gravity effect. *Transport in porous media*, 80(3):431–439, 2009.
- [110] Hywel Rhys Thomas. *A finite element analysis of shrinkage stresses in building materials*. PhD thesis, University College of Swansea, 1981.
- 1055 [111] Neil C Thompson, Shuning Ge, and Gabriel F Manso. The importance of (exponentially more) computing power. *arXiv preprint arXiv:2206.14007*, 2022.
- [112] Gilles Trystram. Modelling of food and food processes. *Journal of Food Engineering*, 110(2):269–277, 2012.
- 1060 [113] Ian Turner and Patrick Perré. A synopsis of the strategies and efficient resolution techniques used for modelling and numerically simulating the drying process. In *Mathematical modeling and numerical techniques in drying technology*, pages 1–82. CRC Press, 1996.
- [114] Ian W Turner. A two-dimensional orthotropic model for simulating wood drying processes. *Applied Mathematical Modelling*, 20(1):60–81, 1996.
- 1065 [115] Ian W Turner and PC Jolly. Combined microwave and convective drying of a porous material. *Drying Technology*, 9(5):1209–1269, 1991.
- [116] IW Turner, JR Puiggali, and W Jomaa. A numerical investigation of combined microwave and convective drying of a hygroscopic porous material: A study based on pine wood. *Chemical Engineering Research and Design*, 76(2):193–209, 1998.
- 1070 [117] Albert J Valocchi. Validity of the local equilibrium assumption for modeling sorbing solute transport through homogeneous soils. *Water Resources Research*, 21:808–820, 1985.
- [118] DA Van Meel. Adiabatic convection batch drying with recirculation of air. *Chemical Engineering Science*, 9(1):36–44, 1958.
- [119] Madhu Vinjamur and Richard A Cairncross. Non-fickian nonisothermal model for drying of polymer coatings. *AIChE Journal*, 48(11):2444–2458, 2002.
- 1075 [120] KM Waananen, JB Litchfield, and MR Okos. Classification of drying models for porous solids. *Drying technology*, 11(1):1–40, 1993.
- [121] L. Wadsö. Describing non-Fickian water-vapour sorption in wood. *Journal of Materials Science*, 29:2367–2372, 1994.
- 1080 [122] Wei Wang, Guohua Chen, and Arun S Mujumdar. Physical interpretation of solids drying: An overview on mathematical modeling research. *Drying Technology*, 25(4):659–668, 2007.
- [123] S. Whitaker. Simultaneous heat, mass and momentum transfer in porous media: a theory of drying. In J. P. Hartnett and T. F. Irvine, editors, *Advances in Heat Transfer*, volume 13, pages 119–203. Elsevier, 1977.
- 1085 [124] S. Whitaker. Coupled transport in multiphase systems: a theory of drying. In Y. I. Cho J. P. Hartnett, T. F. Irvine and G. A. Greene, editors, *Advances in Heat Transfer*, volume 31, pages 1–104. Elsevier, 1998.

- [125] Ran Yang and Jiajia Chen. Mechanistic and machine learning modeling of microwave heating process in domestic ovens: A review. *Foods*, 10(9):2029, 2021.
- 1090 [126] Tjalling J Ypma. Historical development of the Newton–Raphson method. *SIAM review*, 37(4):531–551, 1995.
- [127] Lingfei Zhang, José MF Ferreira, Susana Olhero, Loic Courtois, Tao Zhang, Eric Maire, and Jens Chr Rauhe. Modeling the mechanical properties of optimally processed cordierite–mullite–alumina ceramic foams by x-ray computed tomography and finite element analysis. *Acta Materialia*, 60(10):4235–4246, 2012.
- 1095 [128] Huacheng Zhu, Tushar Gulati, Ashim K Datta, and Kama Huang. Microwave drying of spheres: Coupled electromagnetics-multiphase transport modeling with experimentation. part i: Model development and experimental methodology. *Food and Bioproducts Processing*, 96:314–325, 2015.

## 1100 Appendix A. Macroscopic formulation of coupled heat and mass transfer

This annex describes the comprehensive set of macroscopic equations describing coupled transfer occurring during drying. This set was proposed by [123, 124] and adapted to the case of hygroscopic products with a balance of dry air required to consider the effect of internal pressure [68, 71].

1105 *Moisture conservation*

All water phases are considered in the accumulation term (liquid, vapor and bound). The fluxes includes the liquid velocity driven by the liquid pressure (convection and capillary), the convection of gas, the diffusion of bound water, and the binary diffusion of vapor in air.

$$\frac{\partial (\varepsilon_w \rho_w + \varepsilon_g \bar{\rho}_v^g + \bar{\rho}_b)}{\partial t} + \nabla \cdot (\rho_w \bar{\mathbf{v}}_w + \bar{\rho}_v^g \bar{\mathbf{v}}_g + \bar{\rho}_b \bar{\mathbf{v}}_b) = \nabla \cdot (\rho_g \mathbf{D}_{eff} \cdot \nabla \omega_v) \quad (\text{A.1})$$

1110 *Energy conservation*

The enthalpy conservation includes the enthalpy of all phases in the accumulation terms, the pressure work, and all enthalpy fluxes due to convection of diffusion migrations.

$$\begin{aligned} \frac{\partial}{\partial t} (\varepsilon_w \rho_w h_w + \varepsilon_g (\bar{\rho}_v^g h_v + \bar{\rho}_a^g h_a) + \bar{\rho}_b \bar{h}_b + \varepsilon_s \rho_s h_s - \varepsilon_g p_g) \\ + \nabla \cdot (\rho_w h_w \bar{\mathbf{v}}_w + (\bar{\rho}_v^g h_v + \bar{\rho}_a^g h_a) \bar{\mathbf{v}}_g + h_b \bar{\rho}_b \bar{\mathbf{v}}_b) + \bar{\mathbf{v}}_w \cdot \nabla p_w + \bar{\mathbf{v}}_g \cdot \nabla p_g \\ = \nabla \cdot (\rho_g \mathbf{D}_{eff} (h_v \nabla \omega_v + h_a \nabla \omega_a) + \boldsymbol{\lambda}_{eff} \nabla T) + \varphi \end{aligned} \quad (\text{A.2})$$

In this equation, the term  $\varphi$  accounts for possible volumetric heat sources, for example in the case of high frequency, or microwave heating. The transport of enthalpy due to bound water migration must be treated with care. As the differential heat of sorption depends on the bound water content, the averaged value  $\bar{h}_b$  should be used in the time evolution (accumulation term), whereas the value at  $\rho_b$  ( $h_b$ ) should be used in the migration term, as it is assumed that the less bound water molecules are those likely to migrate.

1120 *Air conservation*

This equation simply considers the accumulation of dry air in the gaseous phase and its migration by convection and diffusion.

$$\frac{\partial (\varepsilon_g \bar{\rho}_a^g)}{\partial t} + \nabla \cdot (\bar{\rho}_a^g \bar{\mathbf{v}}_g) = \nabla \cdot (\rho_g \mathbf{D}_{eff} \nabla \omega_a) \quad (\text{A.3})$$

In these equations, the barycentric mass velocities are from the generalized Darcy's law:

$$\bar{\mathbf{v}}_g = -\frac{\mathbf{K}\mathbf{k}_g}{\mu_g}(\nabla p_g - \rho_g \nabla \psi_g) \quad (\text{A.4})$$

$$\bar{\mathbf{v}}_w = -\frac{\mathbf{K}\mathbf{k}_w}{\mu_w}(\nabla p_w - \rho_w \nabla \psi_g) \quad \text{with} \quad P_w = P_g - P_c(X, T) \quad (\text{A.5})$$

When the bound water flux is expressed using the bound water density as the driving force, the bound water flux takes the following form:

$$\begin{aligned} \bar{\rho}_b \bar{\mathbf{v}}_b &= -\mathbf{D}_b \nabla \bar{\rho}_b = -\rho_0 \mathbf{D}_b \nabla X_b \\ \text{where} \quad X_b &= \min(X, X_{fsp}) \end{aligned} \quad (\text{A.6})$$

*Boundary conditions*

$$\begin{aligned} \mathbf{J}_v|_{x=0^+} \cdot \mathbf{n} &= h_m c M_v \ln \left( \frac{1 - x_\infty}{1 - x_v|_{x=0}} \right) \\ \mathbf{J}_h|_{x=0^+} \cdot \mathbf{n} &= h_h (T|_{x=0} - T_\infty) \\ P_g|_{x=0^+} &= P_{atm} \end{aligned} \quad (\text{A.7})$$

1125 The first boundary equation assumes that only water vapor is exchanged between the product and the surrounding air.

This macroscopic formulation assumes that the porous medium is locally at equilibrium:

**A1** the temperature is the same for all phases  $T_s = T_w = T_g$

1130 **A2** the partial pressure of water vapor inside the gaseous phase is in equilibrium with moisture content  $X$  via  $p_v = p_{vs}(T) \times a_w(T, X)$ , where function  $a_w$  is the sorption isotherm, also called water activity, namely in food science.

Further assumptions allow this set of equations to have a more convenient form:

1135 **A3** the variation in partial densities inside the REV are negligible; therefore, the intrinsic average is equal to the local value  $\bar{\rho}_v^g = \rho_v$  and  $\bar{\rho}_a^g = \rho_a$ ,

**A4** the solid density is assumed to be constant  $\rho_s = \text{constant}$ ,

**A5** the moisture content  $X$  is used to consider the total amount of water present in the porous medium  $\rho_0 X = \varepsilon_w \rho_w + \varepsilon_g \bar{\rho}_v^g + \bar{\rho}_b$  where  $\rho_0 = \varepsilon_s \rho_s$ ,

1140 **A6** the effective diffusivity is expressed as a function of the binary diffusivity of vapor in air:  $\mathbf{D}_{eff} = \mathbf{f} \mathbf{D}_v$ , where  $\mathbf{f}$  is a dimensionless diffusivity tensor (indeed, along one given direction,  $f = 1/\mu$  where  $\mu$  is the vapor resistance ratio used for building materials),

**A7** The effect of pressure variation has a negligible contribution in enthalpy conservation

With these additional assumptions, the set of equations takes the following compact form:

Moisture conservation

$$\rho_0 \frac{\partial X}{\partial t} + \nabla \cdot (\rho_w \bar{\mathbf{v}}_w + \rho_v \bar{\mathbf{v}}_g) = \nabla \cdot (\rho_g \mathbf{f} \mathbf{D}_v \nabla \omega_v + \rho_0 \mathbf{D}_b \nabla X_b) \quad (\text{A.8})$$

Energy conservation

$$\begin{aligned} \frac{\partial}{\partial t} (\varepsilon_w \rho_w h_w + \varepsilon_g (\rho_v h_v + \rho_a h_a) + \overline{\rho_b h_b} + \varepsilon_s \rho_s h_s) + \nabla \cdot (\rho_w h_w \bar{\mathbf{v}}_w + (\rho_v h_v + \rho_a h_a) \bar{\mathbf{v}}_g) \\ = \nabla \cdot (\boldsymbol{\lambda}_{eff} \nabla T + (h_v - h_a) \rho_g \mathbf{f} \mathbf{D}_v \nabla \omega_v + h_b \rho_0 \mathbf{D}_b \nabla X_b) + \varphi \end{aligned} \quad (\text{A.9})$$

Air conservation

$$\frac{\partial (\varepsilon_g \rho_a)}{\partial t} + \nabla \cdot (\rho_a \bar{\mathbf{v}}_g) = \nabla \cdot (\rho_g \mathbf{f} \mathbf{D}_v \nabla \omega_a) \quad (\text{A.10})$$

## 1145 Appendix B. Drying stress formulation

In this annex, small strains are assumed to ease the exposition. In particular, this assumption allows the various contributions to strain to be simply added and the separation of the tangent tensor (the derivative of the displacement field) into pure strain and rotation is straightforward.

1150 As explained in the text, shrinkage is the driving force for drying stress. It is expressed as a strain tensor (the so-called free shrinkage), which is function of the local moisture content. In the case of an isotropic medium, this strain tensor can be expressed as :

$$\bar{\bar{\varepsilon}}^{sh} = f(X(\bar{x}, t)) \cdot R \quad (\text{B.1})$$

1155 where function  $f$  represents the behavior of the product regarding shrinkage (for example shrinkage proportional to the change of free water for clay or to the change of bound water for wood) and  $R$  is the shrinkage coefficient.

The stress development during drying involves additional strain fields tied to specific mechanical behaviors. All these local strain tensors must be added to obtain the total strain tensor:

$$\bar{\bar{\varepsilon}}^{tot} = \bar{\bar{\varepsilon}}^{sh} + \bar{\bar{\varepsilon}}^e + \bar{\bar{\varepsilon}}^{ve} + \bar{\bar{\varepsilon}}^{ms} + \bar{\bar{\varepsilon}}^{pla} \quad (\text{B.2})$$

1160 As a result of the assumption of small displacement, the total strain tensor  $\bar{\bar{\varepsilon}}^{tot}$  is related to the displacement vector  $\bar{u}$  by a simple expression:

$$\varepsilon_{ij}^{tot} = \frac{1}{2} \cdot \left( \frac{\partial u_j}{\partial x_i} + \frac{\partial u_i}{\partial x_j} \right) = \frac{1}{2} (u_{i,j} + u_{j,i}) \quad (\text{B.3})$$

1165 The expression of the memory strain fields should be as close as possible to the real mechanical behavior of the material. As for the transfers, this usually required a complete set of experimentation. For example, the linear viscoelastic creep accounts for the total history of the material using the creep function  $J$ . To be realistic, this function should be activated by moisture content and temperature. In practice, the creep function can be represented by a set of exponential functions, that allows the product's history to be represented by actualized internal variables [66].

$$\varepsilon_{ij}^{ve}(t) = \int_0^t J_{ij}^n(t-t') \cdot \frac{d\sigma_{ij}(x, t')}{dt'} \cdot dt' \quad (\text{B.4})$$

1170 The full problem is usually solved with the displacement field  $u$  as the unknown variable. It includes the balance equation of internal force, written here in a static way, the body force  $f$ , and a suitable set of boundary conditions either in displacement or in the traction vector (force applied at the domain contour). Einstein notation is used in these equations (derivative of variable

indices placed after a comma and implicit summation of indices appearing twice in a single term):

$$\left\{ \begin{array}{l} \varepsilon_{ij}^{tot} = \frac{1}{2}(u_{i,j} + u_{j,i}) \quad \text{over } \Omega \\ \sigma_{ij,j} + \rho f_i = 0 \quad \text{over } \Omega \\ \sigma_{ij} = a_{ijkl}(\varepsilon_{kl}^{tot} - \varepsilon_{kl}^{sh} - \varepsilon_{kl}^{mem}) \quad \text{over } \Omega \\ \sigma_{ij}n_j = T_i \quad \text{on } \Gamma_{T_i} \\ u_i = D_i \quad \text{on } \Gamma_{D_i} \end{array} \right. \quad (\text{B.5})$$

where

$$\begin{aligned} \bar{\varepsilon}^{mem} &= \bar{\varepsilon}^{ve} + \bar{\varepsilon}^{ms} + \bar{\varepsilon}^{pla} \\ \text{and } \forall i, \Gamma_{D_i} \oplus \Gamma_{T_i} &= \Gamma = \partial\Omega \end{aligned} \quad (\text{B.6})$$

1175 Many products are not isotropic : this is the case for most products of biological origin. In such cases, one must account for the difference in behavior along the material directions. Assuming the medium to be orthotropic (anisotropic medium with orthogonal eigen directions), and using the eigen directions  $X, Y, Z$  as basis, the shrinkage takes the following form:

$$\bar{\varepsilon}^{sh} = f(MC(\bar{x}, t)) \cdot \begin{pmatrix} R_{XX} & 0 & 0 \\ 0 & R_{YY} & 0 \\ 0 & 0 & R_{ZZ} \end{pmatrix} \quad (\text{B.7})$$

1180 Similarly, the elastic behavior, expressed by the order 4 tensor  $a_{ijkl}$  in equation B.5, takes the following form.

For the expression of stress as a function of strain :

$$\begin{pmatrix} \sigma_{XX} \\ \sigma_{YY} \\ \sigma_{ZZ} \\ \sigma_{XY} \\ \sigma_{XZ} \\ \sigma_{YZ} \end{pmatrix} = \begin{pmatrix} C_{XX} & C_{XY} & C_{XZ} & 0 & 0 & 0 \\ C_{XY} & C_{YY} & C_{YZ} & 0 & 0 & 0 \\ C_{YZ} & C_{XZ} & C_{ZZ} & 0 & 0 & 0 \\ 0 & 0 & 0 & G_{XY} & 0 & 0 \\ 0 & 0 & 0 & 0 & G_{XZ} & 0 \\ 0 & 0 & 0 & 0 & 0 & G_{YZ} \end{pmatrix} \begin{pmatrix} \varepsilon_{XX} \\ \varepsilon_{YY} \\ \varepsilon_{ZZ} \\ 2\varepsilon_{XY} = \gamma_{XY} \\ 2\varepsilon_{XZ} = \gamma_{XZ} \\ 2\varepsilon_{YZ} = \gamma_{YZ} \end{pmatrix} \quad (\text{B.8})$$

And for the inverse relation (strain as a function of stress):

$$\begin{pmatrix} \varepsilon_{XX} \\ \varepsilon_{YY} \\ \varepsilon_{ZZ} \\ 2\varepsilon_{XY} = \gamma_{XY} \\ 2\varepsilon_{XZ} = \gamma_{XZ} \\ 2\varepsilon_{YZ} = \gamma_{YZ} \end{pmatrix} = \begin{pmatrix} \frac{1}{E_X} & -\frac{\nu_{YX}}{E_Y} & -\frac{\nu_{ZX}}{E_Z} & 0 & 0 & 0 \\ -\frac{\nu_{XY}}{E_X} & \frac{1}{E_Y} & -\frac{\nu_{ZY}}{E_Z} & 0 & 0 & 0 \\ -\frac{\nu_{XZ}}{E_X} & -\frac{\nu_{YZ}}{E_Y} & \frac{1}{E_Z} & 0 & 0 & 0 \\ 0 & 0 & 0 & \frac{1}{G_{XY}} & 0 & 0 \\ 0 & 0 & 0 & 0 & \frac{1}{G_{XZ}} & 0 \\ 0 & 0 & 0 & 0 & 0 & \frac{1}{G_{YZ}} \end{pmatrix} \begin{pmatrix} \sigma_{XX} \\ \sigma_{YY} \\ \sigma_{ZZ} \\ \sigma_{XY} \\ \sigma_{XZ} \\ \sigma_{YZ} \end{pmatrix} \quad (\text{B.9})$$

## Nomenclature

### 1185 Greek Symbols

|             |   |                   |
|-------------|---|-------------------|
| $\epsilon$  | Volume fraction                           | -                 |
| $\Gamma_D$  | Domain boundary with imposed displacement | -                 |
| $\Gamma_T$  | Domain boundary with imposed traction     | -                 |
| $\mu$       | Viscosity                                 | Pa · s            |
| 1190 $\Phi$ | Porosity                                  | -                 |
| $\rho$      | Density                                   | kg/m <sup>3</sup> |
| $\sigma$    | Stress tensor                             | Pa                |
| $\epsilon$  | Strain tensor                             | -                 |
| $\varphi$   | Volumetric heating term                   | W/m <sup>3</sup>  |

### 1195 Roman Symbols

|              |                                |                          |
|--------------|--------------------------------|--------------------------|
| $\mathbf{n}$ | Normal unit vector             | -                        |
| $c_p$        | Heat capacity                  | J/(K · m <sup>3</sup> )  |
| $D$          | Diffusion coefficient          | m <sup>2</sup> /s        |
| $f$          | Dimensionless mass diffusivity | -                        |
| 1200 $h$     | Specific enthalpy              | J/(K · kg)               |
| $h_h$        | Heat transfer coefficient      | W/(K · m <sup>2</sup> )  |
| $h_m$        | Mass transfer coefficient      | m/s                      |
| $K$          | Permeability                   | m <sup>2</sup>           |
| $L_v$        | Latent heat of vaporization    | J/kg                     |
| 1205 $m$     | Mass                           | kg                       |
| $MC$         | Moisture content, dry basis    | -                        |
| $P$          | Pressure                       | Pa                       |
| $q_h$        | Flux density of heat           | W/m <sup>2</sup>         |
| $q_v$        | Flux density of vapor          | kg/(s · m <sup>2</sup> ) |
| 1210 $R$     | Gas constant                   | 8.314 J/(K · mol)        |
| $RH$         | relative humidity              | -                        |
| $T$          | Temperature                    | °C                       |
| $t$          | Time                           | s                        |
| $V$          | Volume                         | m <sup>3</sup>           |
| 1215 $v$     | Velocity                       | m/s                      |
| $X$          | Moisture content, dry basis    | -                        |

### Subscripts

|          |  |
|----------|--|
| $a$      | Air                                      |
| $atm$    | Atmospheric value                        |
| 1220 $e$ | Elastic                                  |
| $eff$    | Effective value at the macroscopic scale |
| $eq$     | Equilibrium                              |
| $g$      | Gaseous                                  |
| $h$      | Heat                                     |
| 1225 $m$ | Mass                                     |
| $ms$     | Mechanosoprif                            |

|      |            |                          |
|------|------------|--------------------------|
|      | <i>pla</i> | Plastic                  |
|      | <i>s</i>   | Solid                    |
|      | <i>sh</i>  | Shrinkage                |
| 1230 | <i>v</i>   | Water vapor              |
|      | <i>vs</i>  | Viscoelastic             |
|      | <i>w</i>   | Wet bulb or liquid water |

**Superscripts**

$\bar{\psi}$  average of variable  $\psi$  over the REV

1235 **Other Symbols**

$\nabla$  Gradient  
 $\nabla \cdot$  Divergence